Physical Mechanisms of the Therapeutic Effect of Ultrasound (A Review)[1]

M. R. Bailey*, V. A. Khokhlova**, O. A. Sapozhnikov**, S. G. Kargl*, and L. A. Crum*

* *Center for Industrial and Medical Ultrasound, Applied Physics Laboratory, College of Ocean and Fishery Science,*
University of Washington, Seattle, Washington, 981056–6698 USA
e-mail: bailey@apl.washington.edu
** *Department of Acoustics, Physics Faculty, Moscow State University,*
Moscow, 119992 Russia
Received November 16, 2002

Abstract—Therapeutic ultrasound is an emerging field with many medical applications. High intensity focused ultrasound (HIFU) provides the ability to localize the deposition of acoustic energy within the body, which can cause tissue necrosis and hemostasis. Similarly, shock waves from a lithotripter penetrate the body to comminute kidney stones, and transcutaneous ultrasound enhances the transport of chemotherapy agents. New medical applications have required advances in transducer design and advances in numerical and experimental studies of the interaction of sound with biological tissues and fluids. The primary physical mechanism in HIFU is the conversion of acoustic energy into heat, which is often enhanced by nonlinear acoustic propagation and nonlinear scattering from bubbles. Other mechanical effects from ultrasound appear to stimulate an immune response, and bubble dynamics play an important role in lithotripsy and ultrasound-enhanced drug delivery. A dramatic shift to understand and exploit these nonlinear and mechanical mechanisms has occurred over the last few years. Specific challenges remain, such as treatment protocol planning and real-time treatment monitoring. An improved understanding of the physical mechanisms is essential to meet these challenges and to further advance therapeutic ultrasound. © *2003 MAIK "Nauka/Interperiodica".*

INTRODUCTION

The core promise of therapeutic ultrasound is the creation of clinical effects within the body without damaging intervening tissue. Broad and diverse therapies have been demonstrated experimentally and, in some applications, utilized clinically. High intensity focused ultrasound (HIFU) is one example. Figure 1 shows the fundamental concept of HIFU applications. In the focused ultrasound field, the acoustic intensity is sufficiently low near the transducer so that tissue is unharmed. In the focal volume, the intensity is much higher and absorption of the acoustic field is significant enough to thermally denature tissue proteins. A handheld transducer positioned on the skin can therefore noninvasively cauterize bleeding or necrose tumors at specific sites deep inside the human body. This article concentrates on HIFU therapy, which includes hemostasis, surgery, and stimulation of the immune response, but also describes the physical mechanisms of two other ultrasound therapies—shock wave lithotripsy (SWL) and ultrasound-enhanced drug delivery. Recent research and development have brought therapeutic ultrasound to the doorstep of widespread clinical application. Further understanding of ultrasound propagation and physical mechanisms of its interaction with tissue provides the key to fulfilling this potential. The goal of this article is to describe the physical mechanisms that both enable and restrict clinical implementation of therapeutic ultrasound. Background is given; treatment limitations are identified; devices are introduced; numerical and experimental research tools are discussed.

BACKGROUND AND MOTIVATION

Pioneering Work

Ultrasound therapy has a long history, and several review articles describes this field [1–9]. Pioneering work in ultrasound therapy was international [7, 8]. In France, in 1917, Langevin observed the death of fish during the development of sonar [9]. In the United States (US), in 1926 and 1927, Woods and Loomis studied the lethal effect of ultrasound on cells, tissues, fish, and frogs. In Germany, in 1938, Ziess first studied the effects of ultrasound on the eye. Lynn *et al.* are generally credited with the invention of focused ultrasound therapy. They built and tested a high-power, focused, ultrasound transducer and identified localized damage without injury to intervening tissue. In the 1940s, Wall *et al.* in the US, 1950s Fry and Fry in the US, and 1960s Oka *et al.* in Japan, developed focused ultrasound for *in vivo* application to the central nervous system. Fry and coworkers began clinical trials in 1956. Simultaneously, in Russia, Burov and Andreevskaya [10] at the

---

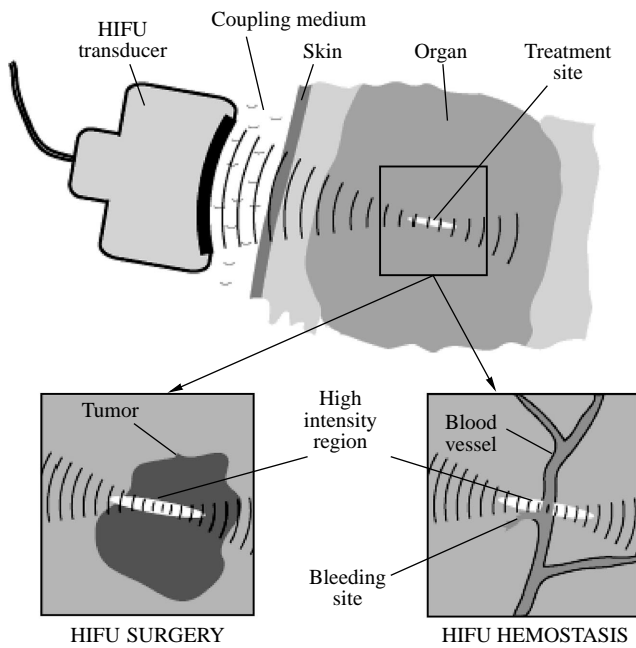[1] This article was submitted by the authors in English.

Fig. 1. The high intensity focused ultrasound (HIFU) beam is focused to necrose a localized tumor region or cauterize a specific bleed without injuring intervening tissue. Acoustic energy distributed over the face of the transducer is concentrated into a volume roughly the size of a grain of rice.

Laboratory of Anisotropic Structures, Academy of Sciences of the USSR were testing somewhat lower intensity, unfocused ultrasound on cancer tumors and found an increased immunological effect. Only recently has much of this work been made public [11]. From these pioneering works, ultrasound has branched into many different treatment areas and types.

Therapeutic Applications of Ultrasound

The clinical applications of ultrasound therapy are broad [2]; however, here, three main categories are defined: (1) high intensity focused ultrasound (HIFU) therapy, which includes tumor necrosis, hemostasis (stopping bleeding caused by trauma or surgical procedure), and immunotherapy; (2) ultrasound-enhanced drug delivery, (3) shock wave lithotripsy (SWL).

The main idea of HIFU therapy, which follows directly from the work of Lynn *et al.* and Fry and Fry, is the use of focused acoustic fields to coagulatively necrose or cauterize tissue [8]. HIFU necrosis has been applied to the brain [12], soft tissue cancers [13–15], benign prostatic hypertrophy (BPH) [16], prostate cancer [17, 18], glaucoma [19], ocular melanoma [20], uterine fibroids [1], fetal surgery [21], myocardial ischemia [3], and many other maladies.

In tumor necrosis, it was found that ultrasound could occlude blood vessels [22] and, subsequently, it has been applied to hemostasis for emergency medical care [23], fetal blood sharing [21], and tumor blood

supply [24]. Likewise, as the direct goal of the work of Burov and Andreevskaya [10] or as a beneficial side effect of HIFU therapy, ultrasound has been shown to induce an enhanced immune response that necroses tumors and protects against new tumor growth [25: Wu *et al.*, pp. 34–43; Marberger *et al.*, pp. 146–153]. It has been shown that ultrasound can enhance the transport of chemicals and genes across biological barriers, such as cells, tissues, and blood clots [2].

Lithotripsy is the use of shock waves to break kidney stones [26–30] or gall stones [31]. In addition, lithotripters are finding new applications in orthopedic medicine [32], such as comminuting calcifications in joints [33].

Although the specific fields of hyperthermia and physical therapy can be classified as therapeutic ultrasound, these fields are not considered in this article because of the low-acoustic intensities typically employed. Ultrasound is commonly used in physical therapy to warm tissues about 1°C. For physical therapy, ultrasound intensities are on the order of 1 W/cm², and treatment times are about 10 min. In hyperthermia, ultrasound is generally not focused; the temperature of a tissue is elevated and held at the level of a threshold temperature (42–43°C) that necroses cancer but not normal cells. The intensities for hyperthermia are on the order of 10 W/cm², and treatment times are 1–2 h. The intensities applied for HIFU are ~1000 W/cm², and tissue is heated to >70°C in 1–3 s. However, the physical mechanism of tissue heating in physical therapy and hyperthermia is the same as in HIFU therapy; hence, as more is learned about HIFU, both of these treatments may benefit. In particular, hyperthermia, which has practically declined due to the problems of temperature control, may undergo a resurgence because of HIFU temperature-monitoring and transducer technology as well as synergistic effects with other treatments such as radiation [3].

Clinical Practice

HIFU. Although much basic research remains to be done, it should be underscored that high intensity therapeutic ultrasound is already in clinical use. Representative clinical applications are summarized here. Currently, the world leader in the clinical application of HIFU is China, where at least three companies exist that manufacture HIFU machines and over 1400 patients have been treated for cancerous tumors in bone and soft tissue [15; 25: Wu *et al.*, pp. 34–43]. Chinese machines have been exported and are being used in liver and kidney cancer treatments in Oxford, England. Prostate cancer is treated in Europe [25: Chaussy *et al.*, pp. 1–7] and Japan [18; 25: Uchida *et al.*, pp. 8–16], and BPH is also treated in the US by HIFU [16]. Two companies produce and sell machines for prostate therapy [25: Chaussy *et al.,* pp. 1–7; Uchida *et al.,* pp. 8–16]. An MRI-guided HIFU machine is produced in

Israel, and MRI-guided HIFU trials are underway for breast cancer [14]. Clinical trials for the treatment of soft tissues continue in Sutton, England without the need for patient anesthetic [13; 25: Allen *et al.*, pp. 17–25]. Ten patients with pancreatic cancer have been treated by an interstitial HIFU device in France [25: Lafon *et al.*, pp. 26–33]. A catheter-based device is used in the US to heat vascular stents to prevent restenosis [34]. Since 1985, HIFU has been used in the US to reduce intraocular pressure produced by glaucoma [8, 35]. In hemostasis, trials are underway for catheter wound closure by HIFU.

Ultrasound-enhanced drug delivery. Human trials are underway in the US for catheter-based ultrasound in conjunction with thrombolytic drugs to accelerate the dissolution of blood clots in the heart. At least two US companies are developing thrombolytic ultrasound devices. In Russia devices are commercially available for intraocular drug delivery [36, 37].

Lithotripsy. Since the early 1980s, lithotripsy has been the most common treatment for kidney stones and continues to be the favored method for uncomplicated, upper urinary tract calculi, even with the advent of percutaneous surgical techniques. Over 40 models of lithotripter models are available. Modified lithotripters are used in the US and Europe to treat plantars fasciitis and epicondylitis.

This list is intended to show that ultrasound therapy is not solely a scientific exercise but it is in expanding clinical use. However, aside from a recent burgeoning in HIFU cancer therapy in China, the treatment of kidney stones is the only therapeutic ultrasound that is in significant use. Nevertheless, by targeting specific injuries or ailments, therapeutic ultrasound is finding increasing clinical application.

Challenges and Pitfalls

Five major challenges to successful clinical implementation of HIFU are discussed here.

Focal gain and acoustic windows. One specific challenge is obtaining large focal gains of acoustic pressure through acoustic windows available in the body to transmit ultrasound. Large gain is needed to insure high intensities only at the focus and to spare intervening tissue. Skin burn is the most common side effect of transcutaneous HIFU treatment, because absorption in the skin is several times higher than internal soft tissue. Acoustic intensities, therefore, must be particularly low when crossing the skin [8]. In addition, efficient acoustic coupling to the skin and cooling of the transducer can eliminate skin burns and are important areas of research engineering. For example, flat transducers are more difficult to focus than curved ones but can be easily coupled by direct contact with the skin. Bones are even more absorptive than skin, so it is important to minimize their exposure to ultrasound and is usually avoided during treatment. Wu *et al.*

[25: p. 34–43] have removed ribs to open acoustic windows for HIFU treatment of the liver, and Fry and Fry [7] removed portions of the skull to access the brain. Clement and Hynynen [12] use high aperture transducers with very large gain to focus through the skull, but must correct for refraction of the acoustic beam. Such a need for correction requires the use of phased arrays for electronic focusing and steering the HIFU beam.

Real-time imaging is a second challenge for diagnosis of the disease, targeting, and monitoring the HIFU. Clinical trials for HIFU treatment of Parkinson's disease had successful outcomes but were stopped because of the difficulty of diagnosing the area to be treated and in monitoring the treatment [8]. In contrast, the HIFU treatment of glaucoma has been accepted clinically because of the simplicity of imaging and targeting, as the treatment site is optically transparent [19]. It should be noted that imaging is the area that has advanced most significantly since the early HIFU experiments. Current researchers can leverage emerging imaging modalities in MRI and ultrasound. However, the following challenges remain: real-time compensation for patient motion, localization of tumors or bleeding sites, and determination of therapy end point such as complete tumor necrosis or kidney stone comminution.

Treatment planning, the choice of optimal parameters of HIFU-transducer and treatment protocol, based on the acoustic parameters for each specific case is a third challenge. Consider, for example, the process of treating a tumor. To set the parameters of treatment for ablation of the tumor and only the tumor, it is necessary to perform theoretical modeling of acoustic and temperature fields in tissue for given amplitude, frequency, and geometry of the HIFU transducer and with account of absorption and refraction of ultrasound and heat diffusion. On the other hand, for modeling, it is necessary to know tissue parameters, which cannot be measured or predicted with high enough accuracy in all situations. Furthermore, the typical lateral size of the beam focal spot is about 1 mm, which is substantially smaller than the size of many tumors, so a method to treat the whole tumor is needed. The process of creating a discrete sequence of small lesions to necrose a large tumor has been used until recent time. However, in some cases, this protocol appeared to be prohibitively long, because without sufficient cooling time between exposures, the lesions become unpredictably distorted in their shape due to the change in acoustic parameters of heated tissue and cavitation [38, 39]. Wu *et al.* [15; 25: p. 34–43] introduced another scheme in order to accelerate HIFU therapy. Instead of a series of individual thermal lesions, Wu *et al.* paint a stripe of lesion as the transducer of much higher intensity is continuously moved. Control of the HIFU treatment in this case is to adjust the ultrasound intensity level based on real-time ultrasound imaging feedback—a hyperecho, a bright spot, which is observed during HIFU treatment at such high intensities. This is the current trend in HIFU tumor

necrosis: to emphasize real-time imaging, not relying only on precise prediction of treatment but on the ability to react to the image as well.

Calibration and optimization. Fundamental study and understanding of the physical mechanisms involved in ultrasound therapy enable optimization of HIFU instrumentation and standardization of protocols for treatment in new therapies. Standards have been developed for calibration of transducers by force balance or hydrophone [40], for cavitation detection [41], ultrasound bioeffects [42], and correction for artifact in temperature measurement by thermocouples [43]. However, further standardization and dosimetry of HIFU is needed [25: ter Haar *et al.*, pp. 307–313]. For example, one of the main characteristic values for HIFU transducers is spatial average intensity I_{SAL} defined as $I_{SAL} = W_*/\pi r_*^2$, where W_* is the acoustic power transmitted through the circle area of radius r_*, which is the lateral beam radius measured in the focal plane at half-maximum pressure level at low intensity in water [44]. However, treatments with the same time-averaged I_{SAL} but different duty cycles yield very different lesions. In some cases, another measure, such as maximum peak pressure, is needed as well to calibrate the treatment. Frequency and F-number (focal length/aperture diameter) are also both necessary to characterize an HIFU source.

Consider, as another example, lithotripsy. One of the standard calibration measures of the lithotripter shock field is the peak positive pressure that should define the maximum mechanical stress on a kidney stone. However, it appears that peak positive pressure does not correlate with effectiveness among different types of machines. Hence, other mechanisms must be considered, such as cavitation, which depends not on the positive but on the negative pressure. It appears also that lithotripsy is an effective treatment for kidney stones but it is not successful to comminute more common gallstones. The reason is that conditions in the gallbladder inhibit the physical mechanisms of shock wave impact on stones. Gallstones are more resistant to brittle failure than kidney stones; the fluid surrounding the stone is more viscous, which suppresses cavitation erosion of the stone; and lastly, the mechanism for removal of stone particles is not as efficient as in the kidney. Hence, although the clinical extension of lithotripsy to gallstones is possible, the same mechanisms are not as effective, and calibration and optimization are specific to this particular application.

Indirect technical influences. Clinical trials and targeted engineering are expensive; therefore, the perceived financial payback must be clear. The following considerations influence the investment in HIFU application and have a strong impact on its development: ease of use, reliability, portability, efficiency and sterilability, competing technologies, money/marketability. Ultrasound for intraoperative hemostasis has some distinct advantages over the current clinical treatment of electrocautery. Electrocautery is restricted to the tissue surface, and surface bleeding reduces the effectiveness of electrocautery. Conversely, ultrasound penetrates beneath the surface, and blood improves the ultrasound coupling. However, water filled coupling housings for the ultrasound transducers are difficult, and, thus, more expensive, to keep sterile than the simple metal spatula electrocautery transducers. These facts drive the engineering of new coupling for HIFU hemostasis [45]. In another example, the number of lithotripsy procedures increased significantly with a small technological advance—the advent of mobile lithotripters—that delivered the treatment to the patients in a way that conventional surgery could not.

Complexity and high cost of the new methods become unimportant when the existing methods are not successful. For example, although it may seem that a tumor can be removed surgically if it can be imaged and localized, this is not always the case. There are inoperable tumors (e.g., many liver metastases and pancreatic tumors) for which HIFU may offer the only treatment option, because it is bloodless, it has low risk of infection, and the procedure can be repeated.

METHODS

Transducer Technology

HIFU. An excellent review of current transducer technology can be found in a recent paper by Cathignol [9]. The transducers used in surgery and hemostasis generally are piezoceramic and operate in the 1−10 MHz frequency range, with 2–4 MHz being the most common, and up to 20 MHz for some applications in the eye. Intensities (I_{SAL}) at the focus range from 1000–10000 W/cm². The most common intensities are around 1500–3000 W /cm², in interstitial applications, intensities are typically lower, but the new clinical Chinese devices operate on the order of 10 000 W/cm². Transducers receive 100–500 W of electrical power with the acoustic output generally limited to a maximum pressure of 2–4 MPa sustainable by simple, unmodified ceramics. F-numbers are approximately one but can be as high as 1.5. Treatment depths are up to 15 cm. Transducers usually operate in periodic pulse regimes being on for seconds and off for tens of seconds. If an HIFU transducer works simultaneously with an ultrasound imaging system, the intense signal introduces a strong noise into the image. To synchronize with the video frame rate of an ultrasound imager, the HIFU driving signal can be gated at about 20 Hz.

Transducers are generally manufactured in the shape of a spherical segment, either as a single curved element or several elements on a curved backing. Figure 2 shows some single element transducers for hemostasis. Elements are made of piezoceramic or piezocomposite material. The piezoceramic can be machined into curved shapes, and the entire surface area is active.

However the characteristic acoustic impedance (33 MRayl) is not well matched to water (1.5 MRayl), so special matching layers are generally used to improve transmission. Parasitic vibration modes are common [46]. Adding backing material behind the element reduces the parasitic modes and increases the bandwidth but decreases the efficiency of the transducer. To make arrays, a piezoceramic must be sectioned.

A piezo-composite is a diced ceramic, where the spaces are filled with a polymer [46]. The composite material can be designed for heat dissipation or structural support. The material can be formed, vibrations are naturally damped, and the structure is inherently designed to be implemented as an array. Compared to piezoceramic, the characteristic acoustic impedance of piezo-composite (10 MRayl) is much closer to that of water, so transmission is more efficient. The piezo-composite also has a high electromechanical coupling factor (0.7); for piezoceramic it is normally less than 0.5. Efficiencies of both piezoceramic and piezo-composite transducers used in HIFU are often 70%. Liquid cooling is often required for interstitial devices but neglected in transcutaneous devices. To treat larger tissue volumes in a minimum treatment time, two approaches have been taken in transducer design: focus aberration and arrays. The focus has been blurred to broaden the treatment area by mechanical vibration of the transducer [47], electrode strips [20], and a split focus design [48]. Arrays offer the ability to steer the HIFU focus or to create simultaneously multiple HIFU foci in order to increase the treatment volume [3, 49, 50]. An HIFU array or a mechanically scanned single-element source [18] can be used for imaging as well as for treatment; however, a separate imaging array is commonly used [1, 17]. Precise manufacturing of the HIFU system is required to isolate each element electrically and acoustically, to prevent overheating, and to integrate a large number of linear amplifiers to properly and finely phase the signals.

Ultrasound-enhanced drug delivery. Frequencies used for ultrasound-enhanced drug delivery are usually around 20 kHz, although 1–2 MHz are also used. Typical intensities are lower, but treatment is longer than in HIFU. Transducers are generally unfocused and less taxed than in HIFU, although miniaturization of catheter devices to target small vessels responsible for strokes presents an engineering challenge. Lithotripters are also used for gene and drug transport [27]. A unique design developed by Kawabata *et al.* for extracorporeal drug delivery is two confocal transducers with two frequencies 0.5 and 1 MHz [25: p. 539–543]. The mixing of these frequencies properly shifted in phase substantially decreases the cavitation threshold and enhances cavitation, which is a primary mechanism in enhancement of drug delivery. Similar results have been recently obtained with mixing high frequency bursts and continuous low frequency ultrasound [25: Bailey *et al.*, pp. 472–480]. Cavitation can be localized in this

Fig. 2. Single element piezoceramic transducers (3–10 MHz) designed for acoustic hemostasis. The circular matching layer and element connect to a 10-cm handle. A detachable water-filled cone provides the acoustic coupling. [Figure courtesy of P.J. Kaczkowski, CIMU, University of Washington.]
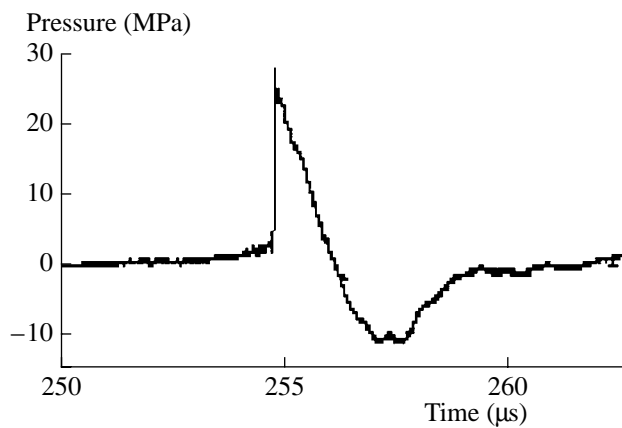

Fig. 3. Waveform measured with a PVDF membrane hydrophone at the focus of an electrohydraulic lithotripter. Characteristically, a positive-pressure spike leads a slightly longer negative pressure trough. Treatment commonly requires about 2000 pulses administered at 1–2 Hz.

case if the higher frequency transducer is focused. The field of manipulating the waveform to control cavitation in therapeutic ultrasound is an emerging one with great potential.

Lithotripsy. Lithotripters produce short focused microsecond pulses as opposed to a burst of many cycles at a characteristic frequency in HIFU. A common lithotripter waveform at focus is shown in Fig. 3. Peak positive pressure is 20–140 MPa and peak negative pressure is –8 to –15 MPa. Thousands of pulses are delivered in a treatment at rates of 1–2 Hz. Electrohydraulic lithotripters are commonly gated to the cardiac cycle because the electrical output can cause arrhythmia. Higher rates would accelerate treatment but cause more tissue injury. Lithotripters are typically tens of centimeters in aperture with F-numbers around one. Acoustic coupling with the patient is achieved through
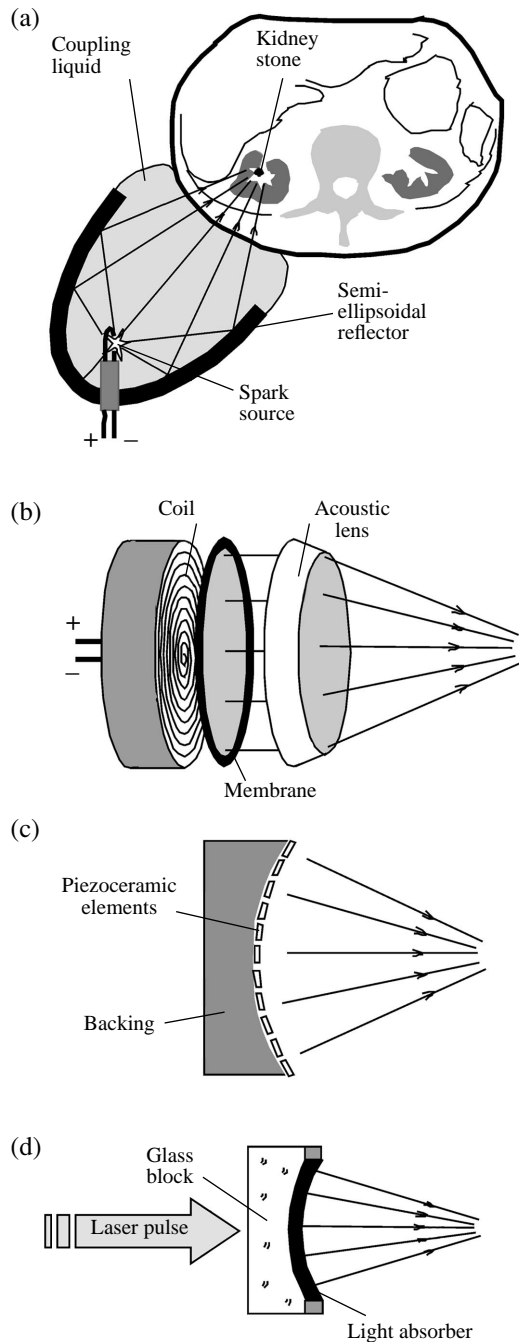
(a)

Coupling liquid

Kidney stone

Semi-ellipsoidal reflector

Spark source

+ −

(b)

Coil

Acoustic lens

+

−

Membrane

(c)

Piezoceramic elements

Backing

(d)

Glass block

Laser pulse

Light absorber

Fig. 4. Three clinical and one research lithotripter designs. Electrohydraulic machines (a) use an ellipsoidal reflector to focus the shock wave generated by an underwater spark. Electromagnetic devices (b) employ impulsive displacement of a plate to generate the wave, which is focused by a lens or reflector. Piezoceramic lithotripters (c) utilize the waves generated by piezoelectric elements. The laser lithotripter (d) relies on the conversion of an optical wave to an acoustic one in a thin spherical layer of a light-absorbing liquid.

water baths or liquid-filled pillows. Finally, orthopedic applications are driving the development of compact designs.

There exist three fundamental types of clinical extracorporeal shock wave lithotripters—electrohydraulic, electromagnetic, and piezoceramic (see Fig. 4). In electrohydraulic lithotripters, an underwater spark generates a shock wave that is focused on the kidney stone by an ellipsoidal reflector. The first and most common lithotripter, the Dornier HM3, is considered the gold standard because of its high long-term stone-free rates (67–90%) for a wide range of stones. New electrohydraulic lithotripters incorporate longer lasting electrodes, which provide repeatable waveforms. Electromagnetic lithotripters conduct high current through a coil, which then repulses a parallel plate. Lenses or reflectors focus the wave created by the displacement of the plate. Piezoceramic lithotripters are generally arrays built on a spherical segment. Array technology allows steering of the beam and even image tracking of the stone. Sufficiently powerful compact devices are being developed with stacked composite elements [51] or electrically prestressed piezoelectric material [9]. Lithotripters are commonly compared on the basis of the product of the peak pressure at the focus and the −6-dB pressure volume, which ranges from 0.2 to 10 cm^3. Since peak pressures are so varied, it might be more logical to compare the volume in which a super-threshold pressure is produced. However, this threshold value has not been determined yet, and a higher product correlates with improved clinical efficacy. Electrohydraulic lithotripters, particularly the HM3, produce low peak pressures (30–40 MPa) but the largest focal volume and the largest product. Newer electromagnetic and piezoceramic lithotripters generally produce more tightly focused beams and higher peak pressures, with the notable exception of the low-amplitude, broad-focused lithotripter developed by Eisenmenger [52]. A fourth type of extracorporeal lithotripter uses a laser source and optoacoustic transduction to generate shock waves (see Fig. 4). A prototype of the laser lithotripter has been built but is not yet used clinically [53]. Sparks, mechanical drills, and lasers are also used intracorporeally to break stones.

New lithotripter research focuses on controlling cavitation. Corresponding methods are to manipulate the timing between pulses [54, 55] or to modify the lithotripter waveform by altering the reflector material in electrohydraulic [56] or electromagnetic devices or reversing the polarity in piezoceramic devices [57].

Numerical Techniques

The goals of theoretical modeling are to better understand ultrasound propagation in tissue, to quantify the interaction of the acoustic field and tissue, and to plan and optimize treatment protocols. Analytical methods yield qualitative estimations, trends, and guides for numerical simulations, which are necessary in most cases. An ideal numerical code must include a model for the nonlinear acoustic field produced by an ultrasound source coupled with models of the main

ultrasound induced phenomena: tissue heating and cavitation. Inclusion of models for streaming, acoustic radiation pressure, shear stresses, reflection, inhomogeneous structure of tissue, and refraction across a liquid–tissue interface may also be necessary; however, calculation time and computational memory place limitations on the complexity of the model. The goal of this section is to describe how each of these effects is simulated and to show their contribution to the acoustic impact on tissue, which will be discussed in more detail in the next section.

Ultrasound field. The Khokhlov–Zabolotskaya–Kuznetsov (KZK) nonlinear evolution equation is widely used to model numerically high intensity acoustic beams [58]. The KZK model has been successfully applied to simulate the acoustic field generated by HIFU [59–61] and lithotripsy sources [62]:

$$\frac{\partial p}{\partial z} - \frac{\beta}{c_0^3 \rho_0} p \frac{\partial p}{\partial \tau} - \frac{b}{2c_0^3 \rho_0} \frac{\partial^2 p}{\partial \tau^2} = \frac{c_0}{2} \int_{-\infty}^{\tau} \Delta_\perp p(\tau') d\tau'. \quad (1)$$

Here, p is the acoustic pressure, z is the coordinate along the beam axis, c_0 is the small-signal sound speed, ρ_0 is the ambient density, $\tau = t - z/c_0$ is the retarded time, β is the coefficient of nonlinearity, b is the dissipative parameter, and $\Delta_\perp$ is the Laplacian operator with transverse coordinates $\mathbf{r} = (x, y)$. The boundary condition $p_0(\tau, \mathbf{r})$ is given at $z = 0$. Equation (1) is the simplest model that provides an adequate description of nonlinear and diffraction phenomena in focused ultrasound beams. The equation accounts for diffraction within a parabolic approximation, while thermoviscous absorption and acoustic nonlinearity are considered within a plane wave approximation. Acoustic nonlinearity is necessary in the model because, at high-pressure levels (typical for HIFU and lithotripsy), it affects thermal and mechanical changes within the tissue. Several modifications of Eq. (1) have been proposed to better fit the frequency power law of absorption found in tissue [59–61, 63, 64] or to more accurately model the diffraction effects [65, 66]. More comprehensive models, based on the solution of Navier–Stokes equations or full wave equations, have been developed recently for lithotripsy and HIFU [67; 25: Curra *et al.*, pp. 275–282].

Various finite-difference algorithms for the solution of Eq. (1) have been developed based on the method of fractional steps with an operator-splitting procedure [68]. The solution is calculated plane by plane along the beam axis z, and, at each Δz step, the diffraction, nonlinearity, and absorption effects are applied sequentially. The algorithms are implemented either in the time domain [62, 69] or in the frequency domain [59–61, 69–73].

In the frequency-domain schemes, the solution to Eq. (1) is represented in the form of a Fourier series expansion

$$p(z, \mathbf{r}, \tau) = \sum_{n=-\infty}^{\infty} C_n(z, \mathbf{r}) \exp(-in\omega_0\tau). \quad (2)$$

Substitution of Eq. (2) into Eq. (1) yields a set of nonlinear, coupled differential equations for the harmonics C_n of the initial signal. Frequency-domain schemes are better suited for modeling cw ultrasound (cancer treatment, hemostasis, drug delivery) and easier to account for frequency dependent absorption in tissue. Time-domain schemes are better for modeling pulsed regimes used in lithotripsy and nonlinear imaging [62, 69]. Specific transformations of the spatial coordinate system are introduced in some algorithms to follow the focused geometry of an acoustic beam [60, 71, 73]. All models can be implemented in two or three dimensions; however, most results have been obtained for two-dimensional axisymmetric beams. Some simulations are available for rectangular ultrasound sources, but these simulations are much more time consuming and have larger memory requirements and, therefore, are still difficult for modeling [74, 75].

The diffraction term, which is on the right-hand side of Eq. (1), is usually solved by either implicit backward or Crank–Nicholson finite difference methods in both the time and the frequency domain [68]. For frequency-domain schemes, implemented not in the form of the complex series of Eq. (2) but in real series, an additional iterative procedure is necessary to obtain the solution [58, 59, 71]. A particular requirement is to perform simulations within reasonably small spatial windows, which results in nonphysical reflections from the transverse boundaries. To avoid this numerical effect, an artificial absorption is introduced within a layer at the edge spatial grids [61, 71]. Some algorithms employ more accurate diffraction operators without the parabolic approximation [65, 66]. In this case, the numerical solution at each z is obtained by the Rayleigh integral. These algorithms are more time consuming; however, they provide more accurate results for strongly focused ultrasound beams.

The absorption term is calculated in the frequency domain based on the exact solution for the amplitude of each harmonic propagating over the distance Δz:

$$C_n(z + \Delta z) = C_n(z) \exp(-\alpha_n \Delta z). \quad (3)$$

Here, $\alpha_n = (n\omega_0)^2 b/2 c_0^3 \rho_0$ is the attenuation coefficient, which exhibits quadratic frequency dependence according to Eq. (1). Attenuation in tissue is nearly linearly dependent on frequency, because relaxation processes dominate thermoviscous heating. In most tissues, attenuation is on the order of 0.1 Np/cm/MHz. The absorption can be easily modified in the frequency domain (3) as $\alpha_n = \alpha_0(\omega/\omega_0)^\eta$ with $1 < \eta < 1.4$. The dispersion is then calculated from local dispersion relationships [64] or minimum phase digital filters [65]. In time-domain algorithms, a finite-difference method is

applied to the absorption term in Eq. (1), as it is proportional to the second derivative [62]. For an arbitrary frequency power law of absorption, this method cannot be used and a convolution is often applied [109]. FFT methods are also used to obtain a solution in the frequency domain and then return to the time-domain formulation at each step [58].

Nonlinear acoustic propagation, the second term in Eq. (1), is implemented in the frequency domain by solving a set of coupled nonlinear equations for harmonics using Runge–Kutta methods. The number of harmonics is up to 1000 for high intensities and shock regimes [61, 76], which makes the algorithms very time consuming even for two-dimensional axisymmetric beams. To decrease the number of harmonics, an artificial viscosity rapidly increasing with frequency is introduced for the last few harmonics [59, 63]. Artificial or numerical absorption of high frequencies and the corresponding smoothing of the shock front may result in an underestimation of the enhanced heating. To avoid the smoothing of the solution, an asymptotic spectral method has been developed to govern shock waves. In this method a relatively small number of the first harmonics is calculated numerically and the higher harmonics are included in the algorithm using a high frequency asymptote of a shock wave spectrum [60, 64]. The asymptote is also employed in the reconstruction of an acoustic waveform from the finite spectrum, calculation of intensity, and heating. Various methods of solving the nonlinear term in Eq. (1) are used in the time-domain schemes. One method uses an exact solution that distorts a uniform time grid and then interpolates the solution back to the initial grid [62, 69]. This method is very stable but introduces an artificial absorption of the solution. An absorption term is also necessary to correctly govern the movement of the shock front. Other finite-differences schemes have been developed that use the method of characteristics [58] or conservation laws [63].

The results of modeling the acoustic field are used to model the thermal and mechanical impact of ultrasound on tissue. Heat sources are calculated from the time-averaged intensity vector $Q = -\nabla \cdot \mathbf{I}$ as $\mathbf{I} = \langle p\mathbf{v} \rangle$ in full-wave equation models or strongly focused beams. In the quasi-plane wave approximation of Eq. (1), the intensity and the heat sources can be written in terms of the harmonic amplitudes, Eq. (3), as

$$I = \langle p^2 \rangle / c_0 \rho_0 = 2 \sum_{n=0}^{\infty} |C_n|^2 / c_0 \rho_0$$

$$\text{and } Q = 4 \sum_{n=0}^{\infty} \alpha_n |C_n|^2 / c_0 \rho_0. \qquad (4)$$

In designing an HIFU source, a useful estimate for Q can be obtained from the case of linear plane-wave propagation. The acoustic power absorbed per unit volume at the depth L in tissue is

$$Q = -dI/dz = 2\alpha I_0 \exp(-2\alpha L), \qquad (5)$$

where I_0 is the initial wave intensity at the entrance to the tissue. This simple expression yields an estimate of an appropriate HIFU frequency for penetration to various treatment depths in the tissue. The maximum heat deposition at the distance L in tissue corresponds to the frequency f with absorption length $\alpha^{-1} = 2L$, which satisfies $\partial Q/\partial\alpha = 2I_0(1 - 2\alpha L)\exp(-2\alpha L) = 0$. This estimate is also valid in the quasi-plane wave approximation for weakly focused acoustic beams.

Various generalizations of the presented modeling scheme and complications should be listed here. The KZK equation is an evolution-type equation; i.e., only one-way wave propagation is assumed. A full-wave formulation is computationally intensive but accurately calculates forward and backward propagation caused by reflection from tissue boundaries, bones, or bubbles (i.e., multiple scattering paths). Multiple reflections can be important for skin overheating. A two-dimensional axisymmetric calculation of heating uniform tissue is on the order of minutes to hours with Eq. (1), and a three-dimensional calculation of heating in layered media with a blood vessel or bubble formation takes on the order of a week with a full-wave code [25: Curra *et al.*, pp. 275–282]. The accuracy depends largely on the accuracy of tissue parameters, which must be obtained from experiments, and on the influence of cavitation bubbles. However, a threshold can be determined below which cavitation is unlikely to occur and, thus, will not complicate the calculation or therapy. Another problem is that heat deposition in tissue is proportional to absorption. However, an experimentally measured attenuation includes both absorption and scattering losses with only approximately known relative contribution of scattering. This uncertainty also decreases the accuracy of modeling.

Temperature field. The mathematical model for temperature elevation in tissue is based on the BioHeat Transfer Equation (BHTE) in which the effects of heat diffusion, blood perfusion, and heat deposition are taken into account [77]:

$$\frac{\partial T}{\partial t} = k\Delta T - \frac{T - T_0}{\tau} + \frac{Q}{c_v}. \qquad (6)$$

Here, t is the time, $T(\mathbf{r}, t)$ is the tissue temperature, T_0 is the equilibrium temperature, $k = K/c_v$ is the local tissue temperature conductivity, K is the heat conductivity, c_v is the heat capacity of a unit volume, and Δ is the Laplacian operator. The absorbed ultrasound energy, Q, is calculated from the KZK equation, a full-wave model, or a bubble dynamics equation. The perfusion time, τ, is of the order of hundreds of seconds and can often be neglected in short (~10 s) HIFU treatments. Figure 5 shows good agreement between measured temperature induced in excised liver and the temperature calculated for liver with Eqs. (1) and (6) [78]. Figure 6 shows the
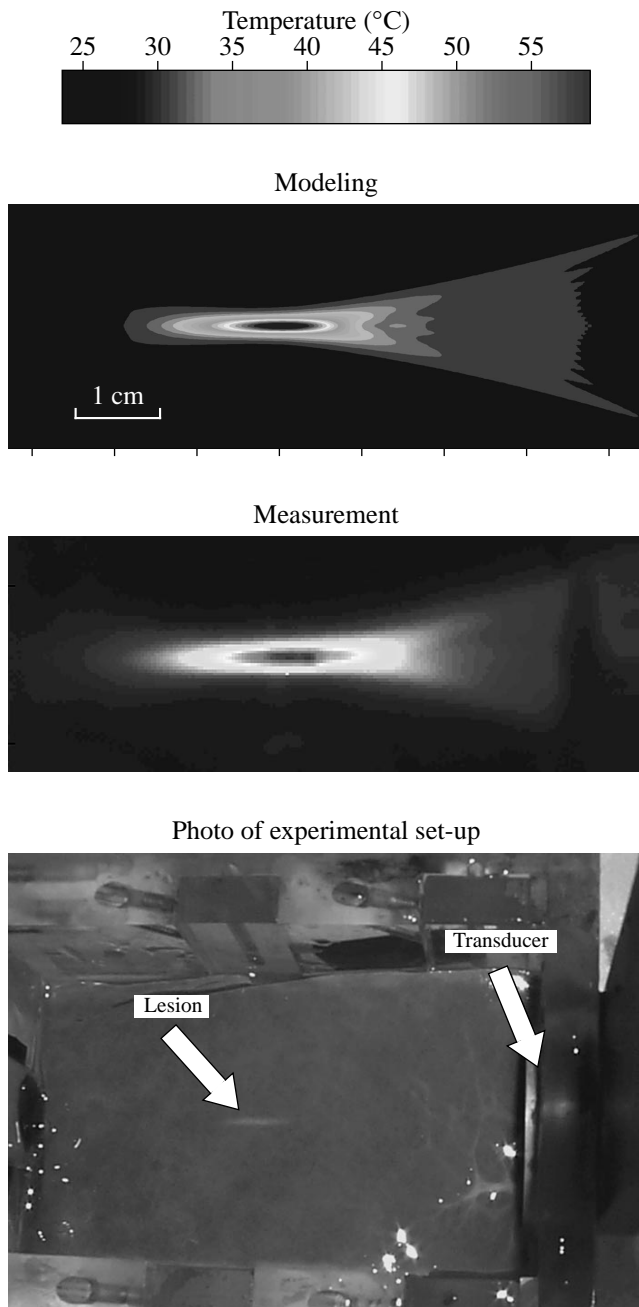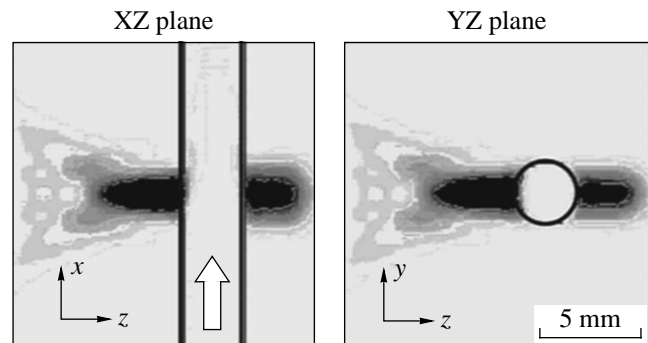
Fig. 6. Numerically simulated tissue temperature near a blood vessel shows that HIFU heating is significant in tissue but advective cooling by blood flow and low absorption in blood keep the interior of the vessel cool. Hence, ruptured vessels can be sealed but remain patent. [Figure courtesy of F. Curra, CIMU, University of Washington.]

Fig. 5. Calculated (top) and measured (center) by infrared camera HIFU-induced temperature rise in tissue. 2-MHz transducer with a 60-W acoustic power, 55-mm focal length, and 35-mm diameter (F-number 1.57) is on the right. For experiment, two layers of bovine liver were stacked along the beam axis. The top layer was immediately removed after 10 s of HIFU exposure, and the thermal image was recorded [78]. The photo of the corresponding lesion is shown at the bottom (white spot).

dose (*TD*) formulation

$$TD_{43°C}(t) = \int_0^t R^{43 - T(t')}dt', \quad (7)$$

with $R = 0.25$ if $T(t) < 43°C$ and 0.5 otherwise [79]. The thermal dose required to create a thermal lesion is equivalent to the thermal dose of a 240-min exposure at 43°C. This definition originated from the hyperthermia protocol, when the tissue was heated to a temperature of 43–45°C in the range during a long exposure of several hours. However, it has been shown that this model gives good estimations of the thermal lesion for the higher temperatures caused by HIFU, which include 10 s at 53°C, 1 s at 57°C, and 0.1 s at 60°C. In HIFU treatments, the temperature commonly exceeds 70°C in about 1–4 s. Thus, tissue necrosis occurs almost immediately.

Cavitation bubble dynamics. In lithotripsy and HIFU, it is common to use cavitation models based on the behavior of a single spherical bubble. These models predict the radial oscillations of a single spherical bubble smaller than the acoustic wavelength and, despite the narrow restrictions of the model, capture the general physics of clusters of bubbles *in vivo* quite well. Most of the single bubble models represent various modifications of the Rayleigh model [80]. For brevity, only the RPNNT (Rayleigh–Plesset–Noltingk–Neppiras–Poritsky) equation is presented here for the radius $R(t)$ of the bubble exposed to ultrasound with an angular frequency ω and peak pressure p_a [80]:

$$R\ddot{R} + \frac{3}{2}\dot{R}^2$$
$$= \frac{1}{\rho}\left[\left(p_0 + \frac{2\sigma}{R_0}\right)\left(\frac{R_0}{R}\right)^{3\gamma} - \frac{4\mu\dot{R}}{R} - \frac{2\sigma}{R} - (p_0 - p_a\sin\omega t)\right]. \quad (8)$$

results of a 3D code to calculate heating near a blood vessel [25: Curra *et al.*, pp. 275–282].

A threshold for thermal necrosis, the denaturing of tissue protein, is calculated according to the thermal
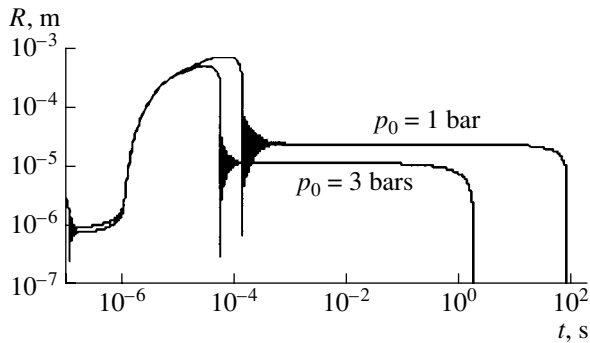
Fig. 7. Calculated radial response of a bubble to a lithotripter pulse for various hydrostatic pressure $p_0 = 1$ and 3 bars. The positive pressure spike (see Fig. 3) of the lithotripter pulse collapses the bubble. The ensuing negative pressure trough initiates growth that continues long after the passage of the lithotripter pulse. Eventually, the pressure difference across the water–bubble interface initiates implosion with strong rebounds. The inertia of the in-rushing fluid that collapses the bubble is sufficiently strong to create shock waves, microjets, and free radicals. Elevated hydrostatic pressure significantly accelerates further dissolution of the bubble.

Here, R, $\dot{R}$, and $\ddot{R}$ are the bubble wall radius, velocity, and acceleration, respectively. The density of the liquid is ρ, p_0 is the external hydrostatic pressure, R_0 is the equilibrium bubble radius, σ is the surface tension, μ is the shear viscosity of the liquid, and γ is the adiabatic exponent of the gas. Equation (8) accounts for the acoustic pressure field that drives the bubble, viscous stresses at the bubble–liquid boundary, and the presence of the gas in the bubble. The Gilmore–Akulichev model is an extension of the RPNNT model, which accounts for the compressibility of the fluid and acoustic radiation [81]. The model has been further modified to include gas diffusion into the bubble [81, 82], evaporation and condensation in the bubble [83], and tissue constraint on the bubble [84]. The numerical solutions to the bubble dynamics equations are obtained with fourth or fifth order Runge–Kutta algorithms with adaptive time steps [68]. Figure 7 shows typical calculated radius-versus-time curves for a 1-μm bubble excited by a lithotripter pulse [82]. The bubble dissolves more quickly at higher hydrostatic pressure.

Coupling of acoustics, temperature, and cavitation. Recent developments in theoretical and numerical models include the interaction of cavitation–temperature–sound effects, complicated structure of acoustic transducers, and the tissue. Bubbles contribute to tissue through the reflection of the acoustic field [59], through nonlinear reradiation [85, 86], and through their motion in a viscous fluid [86, 25: Holt *et al.*, pp. 120–131]. More complicated models have been designed to calculate jet formation [87, 88] or to consider bubble cloud behavior [25: Matsumoto *et al.*, pp. 290–299]. Bubbles can superfocus the acoustic wave by forming a lens and, on the contrary, temperature rise affects sound
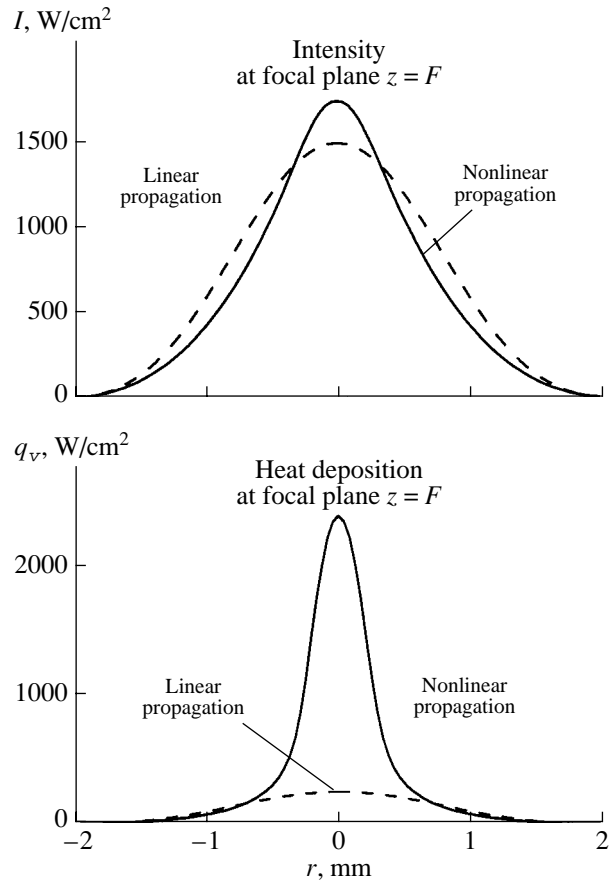

Fig. 8. Focal intensity I and heat deposition q_v versus transverse dimension calculated in liver for a 1.7-MHz transducer with a 15-cm focal length, and 8.4-cm diameter assuming linear and nonlinear propagation [61]. Nonlinear effects predict slightly higher intensities in a slightly narrower focus due to tighter focusing of generated higher harmonic frequencies but predict greatly enhanced heating due to stronger absorption of higher frequencies. Elevated heating efficiency can be achieved through nonlinear acoustic propagation and a judicious selection of peak acoustic amplitude, transducer gain, and duty cycle.

propagation by self-defocusing due to increase of the sound velocity with temperature up to 37–60°C in many soft tissues [89]. In other words, the acoustic parameters of the tissue are temperature and bubble dependent. To compensate for self-defocusing, models of acoustic arrays permit investigation of phase and absorption corrections to predict better locality of the focal spot [90]. Effects of shear can be calculated from the acoustic field and bubble dynamics calculations but as yet are not generally coupled into a dynamic model [91].

Numerical results. Some specific results of numerical modeling are listed here. Nonlinear acoustic models predict a highly localized region of enhanced heating close to the focus. The locally enhanced heat deposition is shown in Fig. 8. An outcome of this result could be lower average power requirements for the same heating predicted linearly by reducing the duty

cycle. Modeling has also described the mechanisms of lesion distortion and migration, specifically, the distortion to a tadpole shape and migration toward the transducer. The following factors are listed in order of increasing contribution to this distortion: nonlinear acoustics, temperature-dependent absorption, and bubbles. The dominant role of bubbles was confirmed by experiment [92, 93]. In SWL, self-refraction, a nonlinear acoustic effect whereby the highest amplitude wave on the axis travels faster and acts to defocus the wave explains why the highest peak pressures are postfocal and the highest peak negative are prefocal [94]. Since negative pressure drives cavitation, and cavitation appears to be an important mechanism in stone comminution, this result might direct where a stone should be positioned in the field [95]. The models also underscore the need for careful determination of tissue parameters and for description of bubble sizes, number of bubbles, vapor or gas content, and effect of tissue constraint on bubble dynamics.

PHYSICAL MECHANISMS

The corner stones of engineering development, numerical simulation, and clinical implementation are the physical mechanisms of the therapeutic effect of ultrasound on biological tissue. The mechanism is critical to design: to increase the likelihood of one mechanism, cavitation, the ultrasound frequency should be lowered; to increase another mechanism, ultrasound absorption, the frequency, in general, should be raised. In addition, the mechanism is crucial to obtaining the desired effect: therapeutic ultrasound is used, in one instance, to stop bleeding and, in another, to reestablish blood flow in clotted arteries. Here, we review some major mechanisms of ultrasound action in different therapeutic procedures.

High Intensity Focused Ultrasound

Absorption. The fundamental physical mechanism of HIFU, ultrasound absorption and conversion to heat, was described by Lele and Pierce in 1972 [96]. Thermal injury is consistent with the coagulative necrosis seen in histology of HIFU treatments [1]. As ultrasound propagates, some energy is absorbed through relaxation and thermoviscous processes and converted to heat [97]. An intrinsic tissue property is that absorption increases nearly linearly with ultrasound frequency; hence, more heating occurs at higher frequencies. However, for transducers with the same F-number, the focus is smaller with higher frequency [98] and penetration depth is also limited by the higher absorption. Equation (5), $\alpha^{-1} = 2L$, defines an optimum frequency for a specific depth. In addition, tissue absorption tends to increase with temperature, especially when the temperature is sufficient to denature proteins. Although complicated by absorption's dependence on temperature, HIFU frequency, and tissue type, we refer to this process as linear absorption, because the heating rate is linearly proportional to the sound intensity (see Eqs. (5) and (6)).

Finite-amplitude acoustics. At high intensity levels, typical for HIFU, ultrasound propagates nonlinearly: the waveform distorts and steep shock fronts develop in the profile. The waveform distortion is synonymous with the production of more rapidly absorbed higher harmonics, which reduces the HIFU intensity and increases the tissue heating [99]. In the case of strong nonlinearity, when shocks are formed close to the transducer, ultrasound can be absorbed before it reaches the focus, leading to overheating of undesirable areas and less focal heating. However, for typical HIFU parameters, nonlinearity is strongly pronounced close to the focus only, which results in enhanced focal heating as strong harmonic production is concentrated and localized [59–61, 72, 99]. The results of numerical simulation of the enhanced temperature rise are shown in Fig. 9. The heating rate is nonlinearly proportional to the HIFU intensity [100]. In fact, waves of the same time-average intensity but different peak pressures and duty cycles produce different heating rates (see Fig. 10).

The amplified heating due to nonlinear absorption is superfocused, which may mean that nonlinear effects play a more significant role during the initial phase, when the thermal lesion is initiated, resulting in a fast excess of the threshold of thermal necrosis in a very small volume, much less than the desired volume of lesion. Later, when the size of the lesion expands over
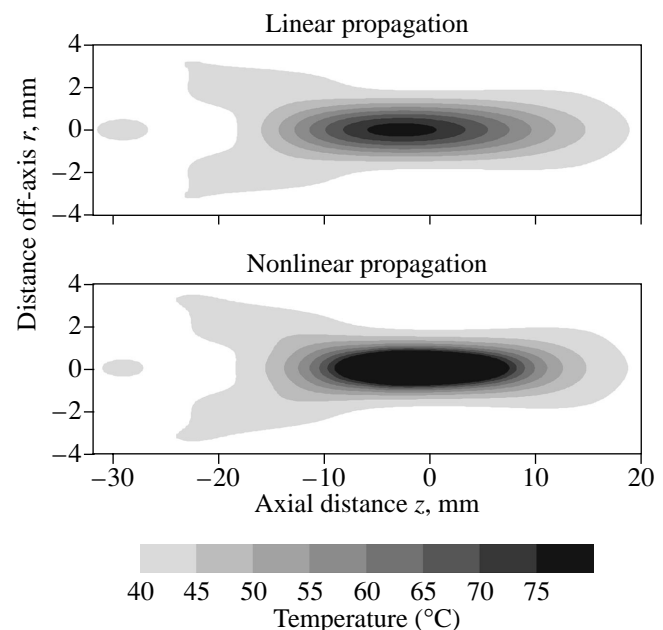
Fig. 9. Numerical simulations of temperature elevation in liver enhanced due to nonlinear acoustics for the same transducer parameters as in Fig. 8. The total volume heated is roughly the same, but the superheating (dark) in the superfocus initiates necrosis sooner and can lead to production of a bubble through boiling.
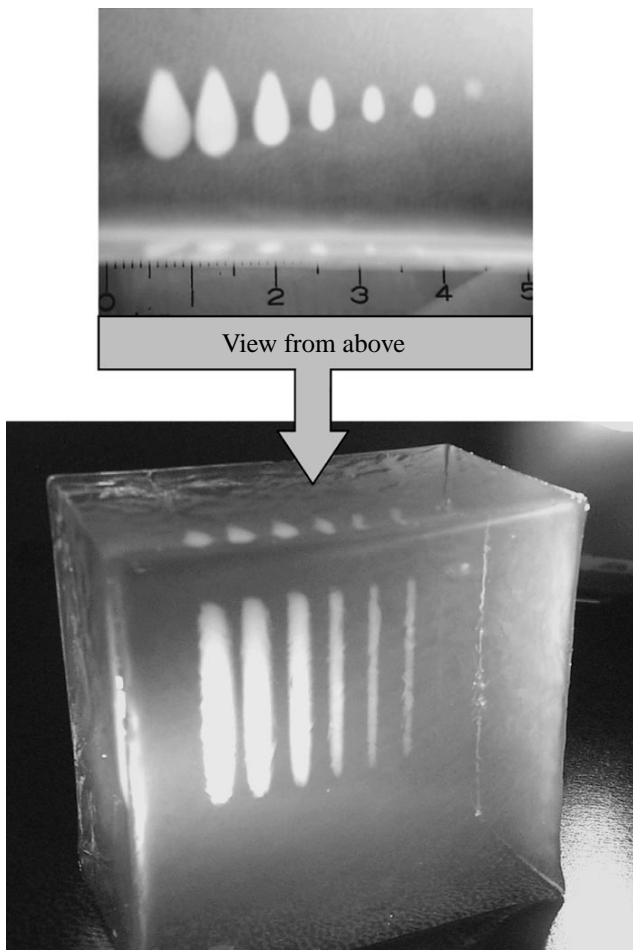
Fig. 10. Top and side view of lesion stripes made by linearly scanning the transducer. The time average intensity is constant, but the duty cycle decreases, the pressure increases, and the lesion increases from right to left due to nonlinear acoustics and cavitation.

timing and degree of collapse is determined by the inertial properties of the surrounding liquid. Inertial collapse is often followed by bubble rebounds.

Bubble formation from nuclei occurs above a threshold that is dependent on pressure (acoustic cavitation), absorbed energy (boiling), and ultrasound frequency. Although formed as primarily vapor cavities, bubbles evolve to contain both gas and vapor, the amount of which varies as the bubble oscillates in the acoustic field. Over large inertial bubble oscillations, such as shown for lithotripsy in Fig. 7, gas diffuses into the bubble and vapor forms by evaporation. In repeated oscillations, bubbles absorb gas and grow by a process of rectified diffusion [102]. When the bubble is large, the gas concentration in the bubble is low and gas diffuses in through a large area and across a thin diffusion skin with rapid change of the dissolved gas concentration. When the bubble is small, the concentration is high and gas diffuses out but through a small area with a thicker diffusion skin. Simulations show that the bubbles grow to a resonant size in the order tens of milliseconds or longer.

Resonant bubble radius depends on the ultrasound frequency. In water, it is approximately $3/f$ μm where the frequency is measured in MHz [80]. In tissue, the resonant radius can be an order of magnitude larger, because tissue constraint makes the bubble stiffer.

Gas softens the bubble collapse by providing stiffness to stop the mass of rushing in water. On the contrary, vapor generally condenses and does not soften collapse by damping the liquid in-rushing to the center of the bubble. However, in lithotripsy, the bubble collapses too quickly for vapor to completely condense, and chemical reactions in the trapped vapor may be significant damping mechanisms [83]. Although bubbles tend toward a resonant size, smaller bubbles are continuously created by bubble fragmentation and dissolution, and larger bubbles may be created by agglomeration.

Bubbles are strong scatterers of ultrasound and, thus, significantly influence HIFU therapy. Bubbles scatter acoustic waves shielding tissue behind a bubble cluster from HIFU energy. Sanghvi *et al.* [5] and others observed that once bubbles form little HIFU penetrates the focus. Bubbles backscatter acoustic waves, causing more energy to be absorbed in the prefocal region before a bubble cluster than that occurring without bubbles. The effect, observed by Watkin *et al.* [39], is the lesion grows wider and toward the transducer as shown in Fig. 11. In practice, the scattering can inhibit therapy if, for example, precisely sized and positioned lesions are planned to completely necrose a tumor volume. On the other hand, scattering from bubbles may enable therapy, in a different HIFU protocol. For example, hemostasis in a tissue volume can be achieved as the lesion propagates toward the transducer in what has been termed a "wall of cautery" [47].
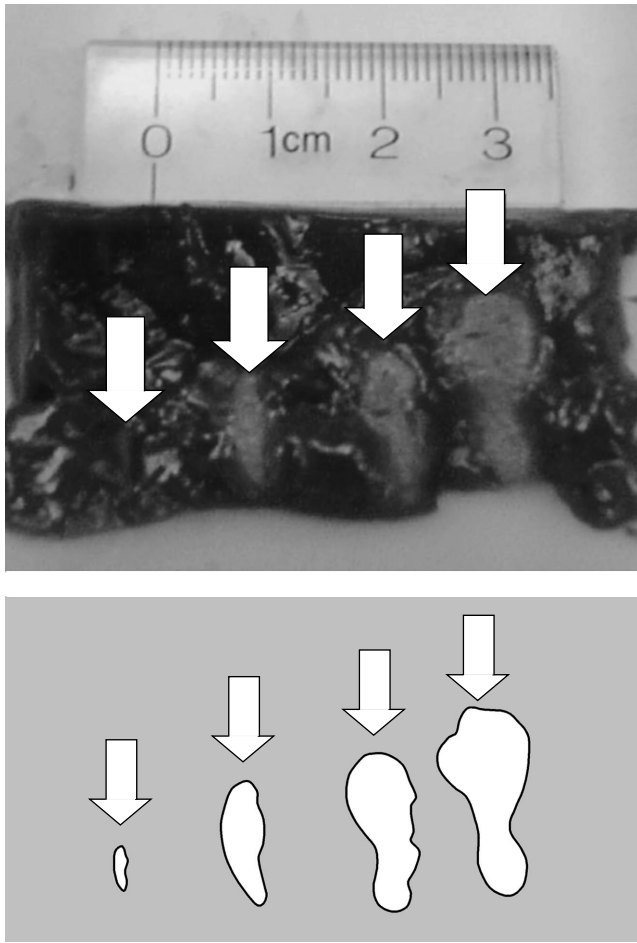
the superheated area, nonlinear absorption is less important if only the thermal mechanism is taken into account. However, if the amplified nonlinear heating is significant, it can accelerate the formation of bubbles and, therefore, initiation of another mechanism of tissue damage—cavitation.

Cavitation damage by HIFU was reported as early as 1930 [101], and a long history makes the case that cavitation (bubble activity) occurs in many HIFU treatments [5, 92]. Bubbles may form from boiling of fluid in blood or tissue or by the growth of tiny cavitation nuclei within the body due to the negative pressure of the acoustic wave. Once initiated, cavitation bubbles oscillate in the acoustic field either noninertially, where the bubbles almost linearly track the pressure changes of the sound field, or inertially, where the bubble dynamics is nonlinear. The change from the negative acoustic pressure to the positive initiates the bubble implosion, and the inertia imparted into the surrounding in-rushing liquid results in bubble collapse. The

Fig. 11. Increasing HIFU intensity (left to right) creates tissue lesions that grow toward the transducer and distort from a symmetric cigar shape to an asymmetric tadpole shape because of scattering from bubbles. Arrows indicate the direction of the axis of the acoustic beam. For better viewing, the lesions are drawn separately in the bottom picture.

Fig. 12. HIFU lesions (left) in transparent gel phantom and B-mode ultrasound images (right) at 1 bar (top) and 100 bars (bottom) static pressure. The lesion is smaller and no hyperecho (arrow) is seen at 100 bar, a sufficiently elevated static pressure to suppress cavitation.

In addition, scattering from bubbles formed in the focal region can be used to image the treatment volume. On B-mode ultrasound, the bubbles appear hyperechoic. Note that overpressure suppresses both the enhanced heating and the hyperecho as shown in Fig. 12 [25: Bailey *et al*., pp. 472–480]. In fact, it has been observed *in vivo* that hyperecho can occur prior to creation of an observable thermal lesion. Thus, at least for some subset of HIFU parameters, the bubbles may precede thermal injury.

It has been observed *in vitro* that a dramatic increase in heating occurs with the appearance of bubbles [86, 25: Holt *et al*., pp. 120–131]. The bubbles themselves cause increased heating due to several mechanisms. First, the energy absorbed by bubbles converts to heat by damping of their oscillation due to viscosity and thermal conductivity inside and close to the bubbles. Second, scattering from bubbles is nonlinear: in addi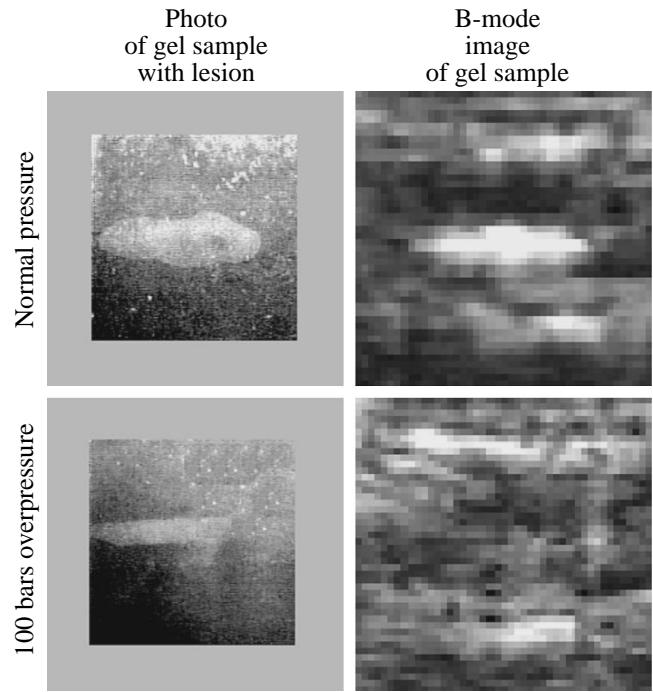tion to the fundamental frequency, the acoustic wave scattered from the bubbles contains higher harmonics that are readily absorbed by the tissue at small distances from bubbles. Bubbles can also be driven to a violent inertial collapse that creates mechanical effects by expansion [104, 105], shock waves [85, 106], microjets [107], and free radicals [108]. Figure 13 shows mechanical tissue disruption at the core of an HIFU lesion in liver.

It has been observed that, in hemostasis, mechanical effects of cavitation emulsify blood and tissue into paste. Radiation force on bubbles slows the bleed (as the transducer axis is commonly opposite the direction of the flow) and drives the paste into the vessel [47]. HIFU heat then cauterizes the paste in place to cover the damage in the vessel. The coagulation cascade can be exited by HIFU when cavitation is present [109].

In tumor treatment, the mechanical effects of cavitation alone, without absorptive heating, can destroy tumor tissue [101]. More recent reports [111] contradict early reports [112] that mechanical effects increase metastasis. In fact, there appears to be an increased resistance to metastasis due to HIFU. It has been proposed that this noninvasive immunotherapy is due to dispersing fragmented antigens into the blood stream that then train the immune system to recognize and attack cancer cells.

Nonthermal, noncavitational mechanisms. Thermal and cavitational mechanisms appear to dominate
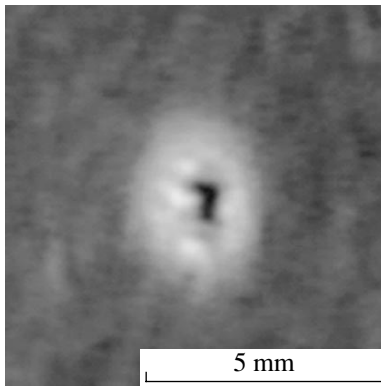
Fig. 13. Mechanical disruption and cavities can be seen at the core of a HIFU-induced lesion in excised liver for sufficiently high exposure intensities or times. Hyperecho, audible acoustic emission, and migration of the lesion often accompany mechanical damage. Cavitation of predominantly vapor bubbles, especially arising in the localized axial region where nonlinear acoustics enhance heating, likely causes the disruption. [Figure courtesy of P.J. Kaczkowski and B.W. Cunitz, CIMU, University of Washington.]

HIFU hemostasis and tumor treatment; however, the mechanisms of a different nature also contribute to HIFU impact on tissue. There is clear documentation of a noncavitational, nonthermal effect on increased immunity to cancer following the treatment. A.K. Burov and coworkers found that, at intensities too low to create thermal lesions ($200 \ \mathrm{W/cm^2}$, small duty cycle), tumors, grown in rabbits from injection of metastatic Brown–Pearce tumor cells, shrunk and even disappeared and that new tumors did not grow following subsequent injection of tumor cells into the vasculature. The same results were seen when animals were treated under elevated hydrostatic pressure to suppress cavitation [10, 11]. Late-stage melanoma tumors were reduced in humans as well. Wu *et al.* have seen a similar immunological effect in shrinkage of tumors not treated directly by HIFU but elsewhere in the body [25: p. 34–43].

It was described above that cavitation fragments cancer cells, releasing material that triggers the immune response. Along with cavitation, pressure gradients resulting directly from the ultrasonic waves may also fragment cells. Although the wavelength of the acoustic waves (usually on the order of 1 mm) is much larger than a cell (8 μm), the shock wave thickness in an ultrasonic wave can be much smaller. In lithotripsy, the shock thickness measured *in vivo* was 150 nm [113]. Hence, a pressure difference on the order of 10 MPa can exist inside a cell and, in addition, the individual components of the cell with differing acoustic impedances are subject to differing forces. These forces can break the cell [11]. Sturtevant and coauthors [29] proposed a mechanism only slightly different for tissue damage by a lithotripter shock wave. The very narrow shock front of the focused wave in fact could be superfocused by inhomogeneities in tissue (what is called

wave front folding in the case of sonic booms propagating in a turbulent atmosphere). This superfocusing creates pressure gradients and shear within cells, tissues, and, in particular, blood vessels. Sturtevant proposed that the shear broke cells. Overpressure experiments in cell suspensions confirm a minimal level of lysis attributed to shear when thermal (in lithotripsy, the pulses are sufficiently short that absorptive heating is negligible) and cavitation effects are suppressed [114]. Ultrasound thus creates shear that yields a nonthermal, noncavitational bioeffect. Note that shear damage *in vivo* may yield pools of blood where cavitation then acts.

Summary of HIFU mechanisms. Chinese clinical success and other evidence establish a number of reasons for working at very high amplitude: faster treatment, increased heating efficiency, and imaging usefulness of bubbles. In fact, in many treatment regimes, bubbles appear unavoidable and may dominate the therapy. Cavitation has been detected at fairly low HIFU amplitudes by harmonic reradiation *in vivo* [115]. Significant heating was measured after cavitation bubbles appeared *in vitro* [86] and *in vivo* [115]. Hyperecho, attributed to bubbles, in some HIFU protocols always accompanies therapy [25: Ebbini p. 280–287] and may precede appearance of a lesion [103]. Numerical simulations show that nonlinear propagation, which results in distortion of waveforms and amplified heating, is inherent in most HIFU protocols [59–61, 72]. According to all these revealed phenomena, the early HIFU paradigm that tissue absorption warms the tissue, the temperature becomes sufficient to denature proteins, the lesion grows through thermal diffusion, and treatment is ceased before increased absorption and heating cause boiling is less accepted now. Instead, it appears more typical that mechanical effects or superheating in a superfocused region due to finite-amplitude propagation of the acoustic wave yields bubbles. Reradiation from the bubbles is a significant mechanism of tissue heating, and the lesion forms after the bubbles. The focus is quickly moved once the lesion has formed to avoid complication caused by bubble scattering. A raster scan pattern of necrotic stripes is painted from the far side of the tumor towards the transducer. The bubbles shield against acoustic penetration and heating beyond the tumor. Throughout, linear and nonlinear mechanisms of absorption are involved simultaneously in heating the tissue.

Lithotripsy

Five stone comminution mechanisms have been studied in lithotripsy. They are erosion [116], spallation [117], dynamic fatigue [29], shear [114], and circumferential compression [52]. These mechanisms may all be activated to differing degrees by either the lithotripter shock pulse or the subsequent collapse of cavitation bubbles excited by the pulse.

Erosion results particularly when bubbles collapse against a surface. In-rushing water is not balanced by

in-rushing water from the direction of the surface, and as a result, a jet of water burrows through the bubble and impinges on the surface. Individual bubbles and bubble clusters create jets, as shown in Fig. 14. Clusters occur in SWL, because the stone exists in a pool of liquid (urine) in the collecting system. It has been calculated that collapses of outer bubbles generate shock waves that force the collapse of the next layer of the cluster, which produces another shock wave, which builds and amplifies toward the cluster center [88].

The shock wave transmitted into the stone when the jet impinges on the stone or the acoustic transmission into the stone of the lithotripter pulse can lead to spallation in the following way. Powerful compression pulse from a lithotripter penetrates into the stone and, after passing to the back surface, reflects from the acoustically soft interface of stone to fluid (the specific acoustic impedance of stones is roughly three to five times higher than that of water or urine). The reflected pulse has an invert polarity; i.e., the powerful compression pulse transforms into a rarefaction pulse of almost the same amplitude. This negative-pressure reflected pulse superimposes with the negative-pressure tail of the incident pulse, creating a high tensile stress and resulting in spallation at some distance close to the back surface of the stone (see Fig. 15). Evidence exists that, without cavitation, spall is reduced or even negated.

Dynamic fatigue is a failure process whereby cracks grow under the repeated compressive and tensile cycles. Commonly, over 1000 lithotripter pulses are used in a treatment, and it is reasonable to expect dynamic fatigue contributes to comminution. The shear mechanism is that described for tissue injury in SWL. Focusing the shock wave can create pressure gradients and, therefore, shear forces within the stone.

Circumferential compression or "squeezing" is the result of the compressive shock pulse traveling faster in the stone than in the surrounding fluid. Hence, at some point, the pulse has traveled through the stone, but ringing the stone is the high pressure of the shock pulse in water, as is seen in Fig. 15. The compressive ring at the equator of the stone produces tensile stress and cracks at its poles.

Compression and spall contribute noticeably when the stone is large. The stones typically are 2–10 mm, bubble clusters reach ~10 mm, the lithotripter pulse is 1–10 mm, bubbles and jets are 1 μm to 1 mm, and the shock front is 150 nm. Research indicates that cavitation is an important factor in lithotripsy [31, 56]: stones initially break by spall, and erosion grinds the fragments into a size suitable for the patient to pass [30]. Simply breaking the stone into pieces is a negative outcome: fragments must be 2 mm or smaller. All these mechanisms may act to varying degrees with different lithotripter and stone types.
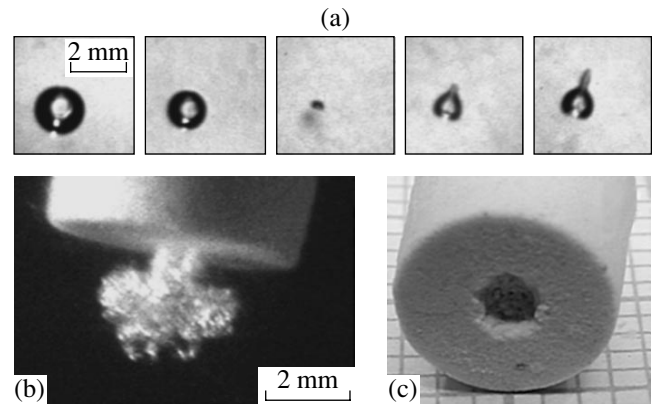
Fig. 14. Jet formation in a single bubble (a) and a bubble cluster (b) due to a lithotripter shock wave. The single bubble (a) excited to 1-mm radius collapses in the third frame and, on rebound, creates a jet of fluid. Frame rate is 20 μs. The cloud that grew to engulf the proximal end of the stone collapses to a mushroom shape (b) as a fluid jet erodes the stone surface (c).
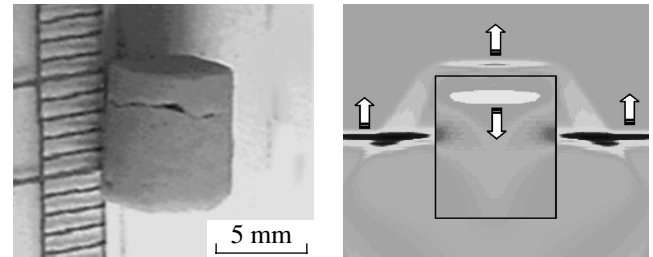

Fig. 15. Calculation of a lithotripter shock wave (pressure shown in dark) traveling up through and around a stone. The pulse moves faster in the stone and reflects and inverts at the distal end. The superposition of the reflection and the trailing negative-pressure trough maximizes the tensile stress at the distal end where the crack is seen in the stone (left). Positive pressure ringing the stone can also cause distal cracking. [Figure courtesy of R.O. Cleveland, Boston University.]

Drug Delivery and Gene Transfection

The primary mechanism of ultrasound-enhanced drug delivery and gene transfection is cavitation [2]. Cavitation microjets puncture holes in cell membranes and convect drugs into cells, tissues, and blood clots. In addition, flow around the oscillating bubble creates compressive, tensile, and shear stress on the biological interface. The flow aids in diffusion through mixing and opens channels by straining membranes.

Control of the cavitation threshold is therefore necessary for drug delivery procedure. It is known that this threshold is lower at lower frequencies because the liquid is under continuous negative pressure for a longer period. A Mechanical Index (peak negative pressure in MPa divided by the square root of frequency in MHz) has been established as the threshold for transient cavitation in diagnostic ultrasound [118]. It is considered
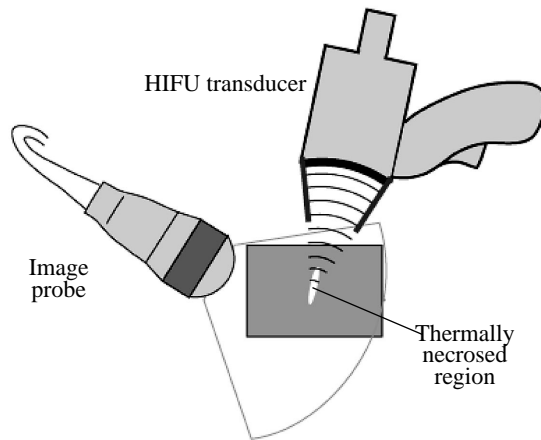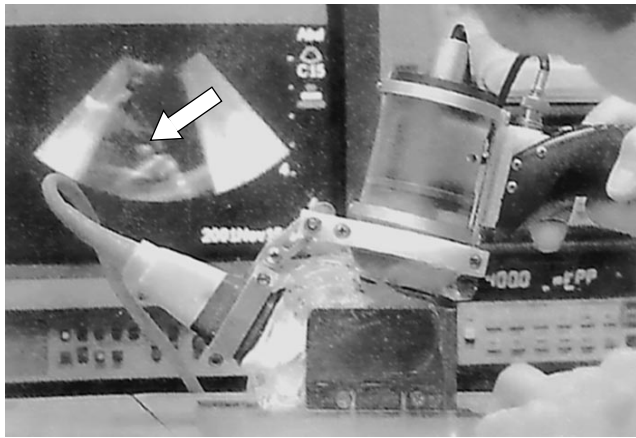
Fig. 16. Acoustic image-guided therapy. The photo of the system is shown on the top, the basic components are repeated at the bottom picture. An HIFU transducer can be translated within a water-filled cylindrical housing to alter the treatment depth. A trigger initiates treatment. Simultaneously, an image probe (left) affixed to the HIFU transducer guides treatment. A bright region (arrow) in the image shown behind corresponds to the thermally necrosed region in the protein/gel phantom.

that the threshold for nonstationary cavitation corresponds to MI = 1, but this is an approximate value. For example, according to MI = 1, 1.6 MPa at 2.5 MHz is the threshold, but measured thresholds in whole blood at 2.5 MHz exceed p_- = 5 MPa [119]. The addition of encapsulated microbubbles greatly reduces the cavitation threshold and increases the cavitation activity [2]. Much of current technology development focuses on developing microbubbles to transport the drug, attach preferentially to the target tissue for example a tumor, and facilitate drug delivery with acoustic cavitation.

Acoustic Image Guidance

The goals of image guidance are diagnosis, targeting, and monitoring of HIFU treatment. The requirement of the real-time imaging in order to target into tissue volume and monitor that bleeding is completely stopped or tissue is coagulated in the target site (and

only there) is unique to HIFU. In particular, compensation must be made for patient motion to avoid treatment of the surrounding tissue.

Fortunately, HIFU produces physical changes of tissue that can be exploited in ultrasound imaging. The fact that these changes take place over the course of the treatment makes reference-frame imaging, where subsequent images are compared to an initial image, and differential imaging, where consecutive frames are compared, useful tools. Changes that can be imaged are bubbles, nonlinear parameter, attenuation, temperature, shear modulus, and displacement of the tissue.

Cavitation/bubbles. The appearance of bubbles in the focal region produces a strong backscatter in the ultrasound imaging signal (see Fig. 12). Figure 16 shows an integrated imaging and treatment system. A hyperechoic region is seen immediately following treatment. It is also possible to image the scattering site during the treatment if HIFU and imaging are synchronized and interlaced in time [103]. The bright spot fades with time (~60 s) as bubbles dissolve and dissipate. If HIFU is ceased at first appearance of the hyperechoic region, no gross tissue injury is observed [103]. This result means that this hyperechoic region can be used to target the treatment area before necrosing tissue.

Nonlinearity. The nonlinear scattering of bubbles can be exploited by imaging techniques developed for microbubble echo contrast agents—second harmonic imaging and pulse inversion. Volterra filtering method has been developed specifically for HIFU [25: Ebbini *et al.*, pp. 280–287]. These methods suppress the linear scattering, which is dominant in tissue, and display other frequencies reradiated by the bubbles. In a slightly different use of nonlinear scattering from bubbles, microbubble contrast agents can be injected into the blood stream following treatment. Areas with blood perfusion become hyperechoic; unperfused regions with lesions give a negative return. Doppler imaging, which displays frequency as color, shows the perfused areas where bubbles produce strong nonlinear scattering. Figure 17 shows (b) B-mode image of the lesion (hyperechoic), (c) power, and (d) directional Doppler images as a contrast agent is injected into the portal vein, and (e) gross histology of the porcine liver lesion. The picture (a) is drawn on the base of (e) and shows the lesion position and size. All modes give a good assessment of the size and shape of the treated region.

Absorption. The absorption coefficient changes under HIFU treatment and this change is particularly large once tissue proteins have denatured. The absorption coefficient can be measured from the backscattered (or transmitted) amplitude versus time. This imaging technique is being developed for clinical implementation.

Temperature. Temperature rise in tissue (even before a lesion has formed) can be measured indirectly by a change of sound speed (travel time) in the tissue [120–122]. With sufficient scatterers in tissue, in either
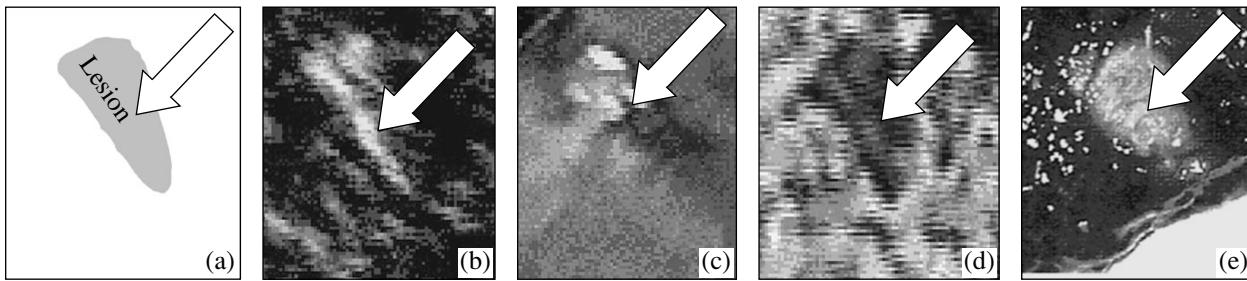
Fig. 17. Three ultrasound images and a gross-histology image of an HIFU lesion in bovine liver. Arrows indicate the lesion. The lesion position and shape are shown in the left picture (a). Hyperecho on B-mode (b) reveals the lesion but fades with time as bubbles dissolve from the lesion. Injection of echo contrast and Doppler mode imaging (c and d) reveal bright colorful signal in areas of healthy blood perfusion and show the necrosed tissue by negative contrast. All images correlated well with the size and shape of the lesion (a and e).

the frequency or time domain, the time between backscattered signals can be tracked and correlated with local sound speed. This technique has shown excellent research results but is not yet used clinically. The challenge appears to be obtaining sufficient scatters and image frames to maintain correlation between frames, especially during rapid heating. The weakness of the method results from the fact that sound speed may increase with temperature until denaturing and then decrease, which gives two values of temperature for a measured sound speed [89].

Shear. The dramatic increase in shear modulus of the lesion due to cross-linked proteins makes the lesion clear in elastography [123, 124] or vibro-acoustography [125, 126]. However, these techniques require modified equipment for applying displacements and detecting the change in backscatter under these displacements. The method is to resolve small displacements in stiff regions, such as the lesion, from large displacements in less stiff tissue by differential imaging with and without an applied force. The skill in elastography is in balancing displacement with imaging frame rate to maintain sufficient coherence between differential frames. Out-of-plane motion is particularly difficult to correct. Displacement can be produced by the HIFU itself and used in imaging [127]. Especially with bubbles in the lesion and the high absorption in necrosed tissue, radiation force is great on the lesion and displacements can be high [25: Lizzi *et al.,* pp. 267–274].

DISCUSSION AND CONCLUSIONS

Therapeutic ultrasound uniquely can treat a specific region in the body without harming surrounding or intervening tissue. Through ultrasound thermal and mechanical effects, activated by specific selections of frequency, amplitude, or waveform, an array of therapies can be affected. In addition, ultrasound can simultaneously provide real-time imaging for diagnosis, targeting, and monitoring of therapy. By targeting specific ailments, therapeutic ultrasound has established a clinical presence, and it has the potential for broad clinical application.

Five technical challenges were identified in order to fulfill the potential of therapeutic ultrasound: acoustic access, real-time imaging, treatment planning, dosimetry, and marketability. Transducer development, such as arrays, is making it possible to obtain high focal gains from existing acoustic windows. Transducers are becoming more powerful, smaller, and more efficient. Numerical modeling is guiding treatment planning. Novel methods of real-time imaging, calibration, and optimization of HIFU devices are being developed.

We suggest that understanding physical mechanisms is an integral to clinical success. The revealing example is the evolution of the concepts on the role of cavitation in lithotripsy and HIFU. Since the mid-1980s, shock wave lithotripsy (SWL) has been a common and effective clinical method to comminute kidney stones. Manufacturers have steadily increased the amplitude of the focus of devices and reduced the focal size in an effort to reduce the required number of shocks and to avoid tissue damage by restricting high acoustic pressures to the stone [28]. However, by many clinical measures, lithotripsy is becoming neither more efficacious nor safer [128, 129], because the designs neglect the mechanism of cavitation. On the other hand, the role of cavitation in HIFU was realized and efforts were made to avoid it. This fear of cavitation and an incomplete understanding of how to work with it have perhaps hindered clinical implementation of HIFU. Until recently, many machines and protocols were designed to heat tissue slowly and avoid cavitation pressure thresholds. Clinical machines currently treating patients in China operate quickly and utilize cavitation for effective tissue necrosis as well as real-time visualization and control of HIFU treatment.

We hope that this paper has given scientists in the other fields the background to apply their expertise to some of the challenges of therapeutic ultrasound.

ACKNOWLEDGMENTS

REFERENCES

1. S. Vaezy, M. Andrew, P. Kaczkowski, and L. Crum, Annu. Rev. Biomed. Eng. **3**, 375 (2001).

2. Echocardiography **18** (4), 309 (2001).

3. C. J. Diederich and K. Hynynen, Ultrasound Med. Biol. **25** (6), 871 (1999).

4. D. J. Coleman, F. L. Lizzi, R. H. Silverman, *et al.*, Ultrasound Med. Biol. **12** (8), 633 (1986).

5. F. J. Fry, N. T. Sanghvi, R. S. Foster, *et al.*, Ultrasound Med. Biol. **21** (9), 1227 (1995).

6. G. ter Haar, Ultrasound Med. Biol. **21** (9), 1089 (1995).

7. K. R. Erikson, F. J. Fry, and J. P. Jones, IEEE Trans. Sonics Ultrason. **21** (3), 144 (1974).

8. N. T. Sanghvi and R. H. Hawes, Exp. Invest. Endosc. **4** (2), 383 (1994).

9. D. Cathignol, in *Nonlinear Acoustics at the Beginning of the 21st Century: Proceedings of 16th ISNA, Moscow, 2002*, Ed. by O. V. Rudenko and O. A. Sapozhnikov (2003), Vol. 1, pp. 371–378.

10. A. K. Burov and G. D. Andreevskaya, Dokl. Akad. Nauk SSSR **106** (3), 445 (1956).

11. V. A. Burov, N. P. Dmitrieva, and O. V. Rudenko, Dokl. Akad. Nauk **383** (3), 101 (2002).

12. G. T. Clement and K. Hynynen, Phys. Med. Biol. **47** (8), 1219 (2002).

13. A. G. Visioli, I. H. Rivens, G. R. ter Haar, *et al.*, Eur. J. Ultrasound **9** (1), 11 (1999).

14. K. Hynynen, O. Pomeroy, D. N. Smith, *et al.*, Radiology **219** (1), 176 (2001).

15. F. Wu, W.-Z. Chen, J. Bai, *et al.*, Ultrasound Med. Biol. **27** (8), 1099 (2001).

16. N. T. Sanghvi, R. S. Foster, R. Bihrle, *et al.*, Eur. J. Ultrasound **9** (1), 19 (1999).

17. A. Gelet, J. Y. Chapelon, R. Bouvier, *et al.*, Eur. Urol. **40** (2), 124 (2001).

18. T. Uchida, N. T. Sanghvi, T. A. Gardner, *et al.*, Urology **59** (3), 394 (2002).

19. P. J. Polack, T. Iwamoto, R. H. Silverman, *et al.*, Invest. Ophthalmol. Visual Sci. **32** (7), 2136 (1991).

20. F. L. Lizzi, C. X. Deng, P. Lee, *et al.*, Eur. J. Ultrasound **9** (1), 71 (1999).

21. M. L. Denbow, I. H. Rivens, I. J. Rowland, *et al.*, Am. J. Obstet. Gynecol. **182** (2), 387 (2000).

22. C. Delon-Martin, C. Vogt, E. Chignier, *et al.*, Ultrasound Med. Biol. **21** (1), 113 (1995).

23. S. Vaezy, R. Martin, G. Keilman, *et al.*, J. Trauma **47** (3), 521 (1999).

24. K. Hynynen, V. Colucci, A. Chung, and F. Jolesz, Ultrasound Med. Biol. **22**, 1071 (1996).

25. *Proceedings of 2nd International Symposium on Therapeutic Ultrasound, Seattle, 2002*, Ed. by M. A. Andrew, L. A. Crum, and S. Vaezy (2003).

26. A. J. Coleman and J. E. Saunders, Ultrasonics **31**, 75 (1993).

27. M. Delius, Eur. Surg. Res. **34** (1–2), 30 (2002).

28. J. A. Moody, A. P. Evan, and J. E. Lingeman, in *Comprehensive Urology*, Ed. by R. M. Weiss, N. J. R. George, and P. H. O'Reilly (Mosby, New York, 2001), pp. 623–636.

29. B. Sturtevant, in *Smith's Textbook of Endourology*, Ed. by A. D. Smith, G. H. Badlani, D. H. Bagley, R. V. Clayman, G. H. Jordan, L. R. Kavoussi, J. E. Lingeman, G. M. Preminger, and J. W. Segura (Quality Medical, St. Louis, MO, 1996), Chap. 39, pp. 529–552.

30. S. Zhu, F. H. Cocks, G. M. Preminger, and P. Zhong, Ultrasound Med. Biol. **28** (5), 661 (2002).

31. M. Delius, F. Ueberle, and S. Gambihler, Ultrasound Med. Biol. **20** (3), 251 (1994).

32. M. Thiel, Clin. Orthop. Relat. Res. **387**, 18 (2001).

33. M. Maier, T. Saisu, J. Beckmann, *et al.*, Ultrasound Med. Biol. **27** (5), 665 (2001).

34. P. J. Fitzgerald, A. Takagi, M. P. Moore, *et al.*, Circulation **103** (14), 1828 (2001).

35. D. J. Coleman, F. L. Lizzi, J. Driller, *et al.*, Ophthalmology **92**, 347 (1985).

36. V. I. Filippenko and V. V. Tret'yak, Voen.–Med. Zh. **8**, 30 (1989).

37. E. I. Sidorenko, V. V. Filatov, and Yu. M. Alimova, Vestn. Oftalmol. **115** (2), 31 (1999).

38. A. L. Malcolm and G. R. ter Haar, Ultrasound Med. Biol. **22**, 659 (1996).

39. N. A. Watkin, G. R. ter Haar, and I. Rivens, Ultrasound Med. Biol. **22**, 483 (1996).

40. *IEEE Guide for Medical Ultrasound Field Parameter Measurements* (IEEE, New York, 1990), IEEE Std 790-1989.

41. ANSI S1.24 TR-2002 American National Standard Technical Report—Bubble Detection and Cavitation Monitoring (2002).

42. J. Ultrasound Med. **19**, 68 (2000).

43. R. L. Clarke and G. R. ter Haar, Ultrasound Med. Biol. **23** (2), 299 (1997).

44. C. R. Hill, Phys. Med. Biol. **15**, 241 (1970).

45. M. Brentnall, R. Martin, S. Vaezy, *et al.*, IEEE Trans. Ultrason. Ferroelectr. Freq. Control **48** (1), 53 (2001).

46. J. Y. Chapelon, D. Cathignol, C. Cain, *et al.*, Ultrasound Med. Biol. **26** (1), 153 (2000).

47. S. Vaezy, R. Martin, P. Kaczkowski, *et al.*, J. Vasc. Surg. **29** (3), 533 (1999).

48. S. Umemura, K. Sasaki, K. Kawabata, *et al.*, in *Proceedings of 1999 International IEEE Ultrasonics Symposium* (IEEE, 1999), Vol. 2, No. 99CH37027, p. 1439.

49. C. A. Cain and S. Umemura, IEEE Trans. Microwave Theory Tech. **34** (5), 542 (1986).

50. L. R. Gavrilov and J. W. Hand, IEEE Trans. Ultrason. Ferroelectr. Freq. Control **47** (1), 125 (2000).

51. J. P. Sferruzza, A. Birer, and D. Cathignol, Ultrasonics **38** (10), 965 (2000).

52. W. Eisenmenger, Ultrasound Med. Biol. **27**, 683 (2001).

53. O. V. Rudenko and O. A. Sapozhnikov, Moscow Univ. Phys. Bull. **46** (1), 5 (1991).

54. P. Zhong and Y. Zhou, J. Acoust. Soc. Am. **110**, 3283 (2001).

55. D. L. Sokolov, M. R. Bailey, and L. A. Crum, J. Acoust. Soc. Am. **110**, 1685 (2001).

56. A. P. Evan, L. R. Willis, B. A. Connors, *et al.*, J. Urol. **168** (4), 1556 (2002).

57. D. Cathignol, J. Tavakkoli, A. Birer, and A. Arefiev, IEEE Trans. Ultrason. Ferroelectr. Freq. Control **45** (5), 788 (1998).

58. N. S. Bakhvalov, Ya. M. Zhileikin, and E. A. Zabolotskaya, *Nonlinear Theory of Sound Beams* (Nauka, Moscow, 1982; AIP, New York, 1987).

59. P. Meaney, M. D. Cahill, and G. R. ter Haar, Ultrasound Med. Biol. **26**, 441 (2000).

60. F. P. Curra, P. D. Mourad, V. A. Khokhlova, *et al.*, IEEE Trans. Ultrason. Ferroelectr. Freq. Control **47**, 1077 (2000).

61. E. A. Filonenko and V. A. Khokhlova, Akust. Zh. **47**, 541 (2001) [Acoust. Phys. **47**, 468 (2001)].

62. M. A. Averkiou and R. O. Cleveland, J. Acoust. Soc. Am. **106**, 102 (1999).

63. T. Christopher, J. Comput. Acoust. **1**, 371 (1993).

64. S. S. Kashcheeva, O. A. Sapozhnikov, V. A. Khokhlova, *et al.*, Akust. Zh. **46**, 211 (2000) [Acoust. Phys. **46**, 170 (2000)].

65. J. Tavakkoli, D. Cathignol, R. Souchon, and O. A. Sapozhnikov, J. Acoust. Soc. Am. **104**, 2061 (1998).

66. P. T. Christopher and K. J. Parker, J. Acoust. Soc. Am. **90**, 488 (1991).

67. S. Ginter, M. Liebler, E. Steiger, *et al.*, J. Acoust. Soc. Am. **111**, 2049 (2002).

68. W. H. Press, S. A. Teukolsky, W. T. Vetterling, and B. P. Flannery, *Numerical Recipes in FORTRAN*, 2nd ed. (Cambridge Univ. Press, New York, 1992).

69. *Nonlinear Acoustics*, Ed. by M. F. Hamilton and D. T. Blackstock (Academic, San Diego, 1998), pp. 66–106.

70. J. Naze Tjotta, S. Tjotta, and E. H. Vefring, J. Acoust. Soc. Am. **89**, 1017 (1991).

71. B. Ystad and J. Bernsten, Acta Acust. (China) **3**, 323 (1995).

72. G. Wojcik, J. Mould, Jr., F. L. Lizzi, *et al.*, in *Proceedings of 1995 Ultrasonics Symposium* (IEEE, 1995), p. 1617.

73. T. Kamakura, T. Ishivata, and K. Matsuda, J. Acoust. Soc. Am. **107**, 3035 (2000).

74. A. C. Baker, A. M. Berg, A. Sahin, and J. Naze Tjotta, J. Acoust. Soc. Am. **97**, 3510 (1995).

75. T. Kamakura, M. Tani, Y. Kumamoto, and K. Ueda, J. Acoust. Soc. Am. **91**, 3144 (1992).

76. V. A. Khokhlova, R. Souchon, J. Tavakkoli, *et al.*, J. Acoust. Soc. Am. **110**, 95 (2001).

77. H. H. Pennes, J. Appl. Physiol. **1**, 93 (1948).

78. V. A. Khokhlova, N. Miller, R. Ollos, *et al.*, in *Proceedings of 17th International Congress on Acoustics* (Rome, 2001), p. 186.

79. S. Sapareto and W. Dewey, J. Radiat. Oncol. Biol. Phys. **10** (6), 787 (1984).

80. V. A. Akulichev, in *High-Intensity Ultrasonic Fields*, Ed. by L. D. Rozenberg (Nauka, Moscow, 1968; Plenum, New York, 1971).

81. C. C. Church, J. Acoust. Soc. Am. **86**, 215 (1989).

82. O. A. Sapozhnikov, V. A. Khokhlova, M. R. Bailey, *et al.*, J. Acoust. Soc. Am. **112**, 1183 (2002).

83. T. J. Matula, P. R. Hilmo, B. D. Storey, and A. J. Szeri, Phys. Fluids **14** (3), 913 (2002).

84. Z. Ding and S. M. Gracewski, J. Acoust. Soc. Am. **96** (6), 3636 (1994).

85. F. Chavrier, J. Y. Chapelon, A. Gelet, and D. Cathignol, J. Acoust. Soc. Am. **108**, 432 (2000).

86. R. G. Holt and R. A. Roy, Ultrasound Med. Biol. **27** (10), 1399 (2001).

87. J. E. Field, Phys. Med. Biol. **36**, 1475 (1991).

88. A. Philipp, M. Delius, C. Scheffczyk, *et al.*, J. Acoust. Soc. Am. **93**, 2496 (1993).

89. J. C. Bamber and F. Dunn, in *Encyclopedia of Acoustics*, Ed. by M. J. Crocker (Wiley, New York, 1997), Vol. 3, pp. 1699–1726.

90. Y. Y. Botros, J. L. Volakis, P. VanBaren, and E. S. Ebbini, IEEE Trans. Biomed. Eng. **44** (11), 1039 (1997).

91. M. Lokhandwalla and B. Sturtevant, Phys. Med. Biol. **46** (2), 413 (2001).

92. P. P. Lele, in *Ultrasound: Medical Applications, Biological Effects and Hazard Potential*, Ed. by M. H. Repacholi, M. Grandolfo, and A. Rindi (Plenum, New York, 1986), pp. 275–306.

93. M. R. Bailey, L. N. Couret, O. A. Sapozhnikov, *et al.*, Ultrasound Med. Biol. **27**, 696 (2000).

94. O. A. Sapozhnikov, Akust. Zh. **37**, 760 (1991) [Sov. Phys. Acoust. **37**, 395 (1991)].

95. D. L. Sokolov, M. R. Bailey, L. A. Crum, *et al.*, J. Endourol. **16** (10), 709 (2002).

96. P. Lele and A. Pierce, in *Proceedings of Workshop on Interaction of Ultrasound and Biological Tissues, Seattle* (DHEW, Washington, 1972), No. 73-8008, p. 121.

97. W. J. Fry, J. Acoust. Soc. Am. **22**, 867 (1950).

98. H. T. O'Neil, J. Acoust. Soc. Am. **21**, 516 (1949).

99. O. V. Rudenko, Moscow Univ. Phys. Bull., No. 6, 18 (1996).

100. O. A. Sapozhnikov, T. V. Sinilo, and Yu. A. Pishchalnikov, in *Nonlinear Acoustics at the Turn of the Millennium: Proceedings of 15th International Symposium on Nonlinear Acoustics, Goettingen, Germany, 1999*, Ed. by W. Lauterborn and T. Kurz (Am. Inst. of Physics, 2000), pp. 483–486.

101. F. O. Schmitt and B. Uhlemeyer, Proc. Soc. Exp. Biol. Med. **27**, 626 (1930).

102. L. A. Crum and G. M. Hansen, Phys. Med. Biol. **27**, 413 (1982).

103. S. Vaezy, X. Shi, R. W. Martin, *et al.*, Ultrasound Med. Biol. **27**, 33 (2000).

104. E. L. Carstensen, D. S. Campbell, D. Hoffman, *et al.*, Ultrasound Med. Biol. **16**, 687 (1990).

105. P. Zhong, Y. Zhou, and S. Zhu, Ultrasound Med. Biol. **27**, 119 (2001).

106. A. Vogel and W. Lauterborn, J. Acoust. Soc. Am. **84**, 719 (1988).

107. L. A. Crum, in *Proceedings of Ultrasonics Symposium* (1982), Vol. 1, p. 1.

108. T. R. Morgan, V. P. Laudone, W. D. Heston, *et al.*, J. Urol. **139**, 186 (1988).

109. S. L. Poliachik, W. L. Chandler, P. D. Mourad, *et al.*, Ultrasound Med. Biol. **27** (11), 1567 (2001).

110. J. Tavakkoli, A. Birer, A. Arefiev, *et al.*, Ultrasound Med. Biol. **23** (1), 107 (1997).

111. J.-Y. Chapelon, J. Margonari, F. Vernier, *et al.*, Cancer Res. **52**, 6353 (1992).

112. F. J. Fry and L. K. Johnson, Ultrasound Med. Biol. **4**, 337 (1978).

113. R. O. Cleveland, D. A. Lifshitz, B. A. Connors, *et al.*, Ultrasound Med. Biol. **24**, 293 (1998).

114. M. Lokhandwalla, J. A. McAteer, J. C. Williams, Jr., and B. Sturtevant, Phys. Med. Biol. **46** (4), 1245 (2001).

115. K. Hynynen, Ultrasound Med. Biol. **17** (2), 157 (1991).

116. A. J. Coleman, J. E. Saunders, L. A. Crum, and M. Dyson, Ultrasound Med. Biol. **13**, 69 (1987).

117. C. Chaussy, W. Brendel, and E. Schmiedt, Lancet **2** (8207), 1265 (1980).

118. R. E. Apfel and C. K. Holland, Ultrasound Med. Biol. **17** (2), 179 (1991).

119. C. X. Deng, Q. Xu, R. E. Apfel, and C. K. Holland, Ultrasound Med. Biol. **22** (7), 939 (1996).

120. R. Seip and E. S. Ebbini, IEEE Trans. Biomed. Eng. **42** (8), 828 (1995).

121. R. Maass-Moreno, C. A. Damianou, and N. T. Sanghvi, J. Acoust. Soc. Am. **100**, 2522 (1996).

122. M. Ribault, J.-Y. Chapelon, D. Cathignol, and A. Gelet, Ultrason. Imaging **20** (3), 160 (1998).

123. R. Souchon, L. Soualmi, M. Bertrand, *et al.*, Ultrasonics **40**, 867 (2001).

124. X. Shi, R. W. Martin, D. Rouseff, *et al.*, Ultrason. Imaging **21** (2), 107 (1999).

125. M. Fatemi and J. F. Greenleaf, Proc. Natl. Acad. Sci. USA **96** (12), 6603 (1999).

126. E. E. Konofagou, J. Thierman, T. Karjalainen, and K. Hynynen, Ultrasound Med. Biol. **28** (3), 331 (2002).

127. O. V. Rudenko and A. P. Sarvazyan, Crit. Rev. Biomed. Eng., No. 3, 6 (2000).

128. J. E. Lingeman, Urol. Clin. North Am. **24**, 185 (1997).

129. J. J. Rassweiler, C. Renner, C. Chaussy, and S. Thuroff, Eur. Urol. **39** (2), 187 (2001).